Near-threshold scattering, quantum reflection, and quantization in two dimensions

Florian Arnecke, Harald Friedrich, and Patrick Raab
Physik Department, Technische Universität München, 85747 Garching, Germany
(Received 18 August 2008; published 24 November 2008)

We study the near-threshold behavior of scattering phase shifts, quantum reflection amplitudes, and quantization functions for systems described by a circularly symmetric potential in two spatial dimensions. In contrast to the three-dimensional case, the centrifugal potential $(m^2-\frac{1}{4})\hbar^2/(2Mr^2)$ is nonvanishing and even attractive for s waves, $m=0$, and the leading near-threshold energy dependence of phase shifts and amplitudes for scattering and quantum reflection is logarithmic in this case. The near-threshold behavior of the s-wave phase shifts and amplitudes can nevertheless be characterized by a well-defined scattering length (for potentials falling off faster than $1/r^2$) and an effective range (for potentials falling off faster than $1/r^4$). For a potential with a bound state at energy $E_n=-\hbar^2\kappa_n^2/(2M)$ very near threshold, the scattering length obeys $a \overset{\kappa_n\to 0}{\sim} 2e^{-\gamma_E}/\kappa_n+O(\kappa_n)$, with no term of order κ_n^0—in contrast to the three-dimensional case. Analytical results are derived for homogeneous potentials, and the necessary modification of the effective-range expansion is given for potentials proportional to $1/r^4$. For $m\neq 0$ we give analytical expressions for the near-threshold behavior of phase shifts as well as scattering and quantum reflection amplitudes, which are generally valid, even when m is neither integer nor half-integer.

DOI: 10.1103/PhysRevA.78.052711 PACS number(s): 03.65.Nk, 34.50.−s, 03.75.−b

I. INTRODUCTION

Interest in two-dimensional scattering theory has been motivated by experiments involving atoms adsorbed to surfaces [1,2]. A two-dimensional theory is, however, not only relevant for planar problems, but also for three-dimensional systems with translational invariance in one of the three directions, as is, e.g., the case for scattering of an atom or molecule by a wire or nanotube. Considerable attention has recently been given to the case of a neutral atom or molecule interacting with an electrically charged wire or nanotube [3,4], where the potential has a strong attractive tail proportional to $-1/r^2$ at large distances. For a neutral wire or nanotube, the interaction potential falls off more rapidly at large distances, but the strength of the centrifugal potential in two dimensions is given by $m^2-1/4$, $m=0,\pm 1,\pm 2\ldots$, so it is always nonvanishing, even for s waves $(m=0)$, where it has the counterintuitive feature of being attractive [5,6]. This attractive centrifugal term in the s-wave radial equation is, on its own, just too weak to support a dipole series of bound states [7], but it does significantly affect the near-threshold behavior of the s-wave scattering phase shift and of the scattering cross section [8–10]. Verhaar *et al.* [11] showed that the concepts of scattering length and effective range can be sensibly used to describe the leading and next-to-leading terms in the near-threshold expansion of the cotangent of the s-wave scattering phase shift for circularly symmetric potentials of finite range, even though the expansion contains a logarithmic divergence in contrast to the well-behaved nature of the corresponding expansion in three dimensions. In this paper we extend the concepts of effective-range theory for scattering in two spatial dimensions to the case of quantum reflection, where the Schrödinger equation is solved with incoming boundary conditions at small distances [12–14]. This provides a realistic description of, e.g., cold-atom scattering, when the atoms are lost from the elastic channel due to inelastic reactions or adsorption at the surface of the scatterer. We also apply a subthreshold version of effective-range theory to derive the leading behavior of the quantization function governing near-threshold quantization and we formulate a relation connecting the s-wave scattering length and the energy of a near-threshold bound state, as recently done for s waves in three dimensions in [15,16].

After a review of the essential features of near-threshold scattering theory in two dimensions (Sec. II), Sec. III describes the adaptation of this theory to the case of quantum reflection by an attractive potential tail and shows how a few characteristic parameters of the potential tail determine the near-threshold behavior of the quantum reflection amplitude, namely, the complex scattering length $\mathfrak{a}$ and the complex effective range $\mathfrak{r}_{\mathrm{eff}}$, which describe the leading and next-to-leading behavior of the complex phase shift $\mathfrak{d}$. In Sec. IV we study quantization in a potential well with an attractive tail and derive the leading behavior of the quantization function that defines the quantization rule near threshold. This leads to a relation which contains the modulus and phase of the complex scattering length $\mathfrak{a}$ and directly connects the real s-wave scattering length a with the energy of a near-threshold bound state as shown in Sec. V.

Section VI is devoted to potentials with homogeneous tails, proportional to $1/r^\alpha$, and gives analytical expressions as well as numerical values for the parameters $\mathfrak{a}$ and $\mathfrak{r}_{\mathrm{eff}}^2$. The special case $\alpha=4$, where the effective-range expansion has to be modified, is treated in Sec. VII.

Nonvanishing values of m are treated in Sec. VIII. We give analytical expressions for the leading and next-to-leading contributions to the near-threshold behavior of the real and complex phase shifts determining the amplitudes for scattering and quantum reflection by homogeneous potentials. The formulas in Sec. VIII are quite general and also applicable when m is not integer or half integer.

II. SCATTERING THEORY AND EFFECTIVE-RANGE EXPANSION IN TWO DIMENSIONS

Relatively detailed descriptions of two-dimensional scattering theory can be found, e.g., in [8–10]. In this section we briefly review some of the main aspects, including the definition of a well-defined scattering length for all potentials falling off faster than $1/r^2$ asymptotically, and of an effective-range term which is well defined for all potentials falling off faster than $1/r^4$.

For a particle of mass M moving in a plane under the influence of the circularly symmetric potential $U(r)$, the stationary Schrödinger equation at energy $E=\hbar^2k^2/(2M)$ is solved by the wave function

$$\psi(\vec{r}) = \sum_{m=-\infty}^{+\infty} \frac{u_m(r)}{\sqrt{r}} e^{im\theta}, \tag{1}$$

when the radial wave functions u_m obey the respective radial Schrödinger equation

$$\frac{d^2u_m}{dr^2} + \left[k^2 - \frac{m^2-1/4}{r^2} - \frac{2M}{\hbar^2}U(r)\right]u_m(r) = 0, \tag{2}$$

which does not depend on the sign of the angular momentum quantum number m. Equation (2) corresponds to the familiar radial Schrödinger equation in three dimensions if we write $l(l+1)$ for $m^2-\frac{1}{4}$, i.e., if we interpret $|m|$ as $l+\frac{1}{2}$. The regular solution c_m and the irregular solution s_m of the free equation ($U\equiv 0$) are given via cylindrical Bessel functions [17],

$$c_m(kr) = \sqrt{\frac{\pi}{2}kr}J_{|m|}(kr), \quad s_m(kr) = \sqrt{\frac{\pi}{2}kr}Y_{|m|}(kr), \tag{3}$$

and their asymptotic behavior is

$$c_m(kr) \overset{kr\to\infty}{\sim} \cos\left(kr - |m|\frac{\pi}{2} - \frac{\pi}{4}\right),$$

$$s_m(kr) \overset{kr\to\infty}{\sim} \sin\left(kr - |m|\frac{\pi}{2} - \frac{\pi}{4}\right). \tag{4}$$

Their behavior at small distances is

$$c_m(kr) \overset{kr\to 0}{\sim} \frac{\sqrt{\pi}}{\Gamma(|m|+1)}\left(\frac{kr}{2}\right)^{(1/2)+|m|},$$

$$s_{m\neq 0}(kr) \overset{kr\to 0}{\sim} -\frac{\Gamma(|m|)}{\sqrt{\pi}}\left(\frac{kr}{2}\right)^{(1/2)-|m|},$$

$$s_{m=0}(kr) \overset{kr\to 0}{\sim} \sqrt{\frac{2}{\pi}kr}\left[\ln\left(\frac{kr}{2}\right) + \gamma_E\right], \tag{5}$$

where $\gamma_E=0.577\,215\,664\,9\ldots$ is Euler's constant. The regular solution $u^{(k)}_{\mathrm{reg},m}$ of Eq. (2) obeys $u^{(k)}_{\mathrm{reg},m}(0)=0$ and is a superposition of c_m and s_m at large distances,

$$u^{(k)}_{\mathrm{reg},m} \overset{r\to\infty}{\propto} c_m\cos\delta_m - s_m\sin\delta_m$$
$$\overset{r\to\infty}{\to} \cos\left(kr - |m|\frac{\pi}{2} - \frac{\pi}{4} + \delta_m\right)$$
$$\propto e^{-ikr} - (-1)^{|m|}ie^{2i\delta_m}e^{+ikr}. \tag{6}$$

If the potential is not too long ranged (as clarified below), then at a given large distance r, the near-threshold behavior of $u^{(k)}_{\mathrm{reg},m}$ follows from Eq. (5) as

$$u^{(k)}_{\mathrm{reg},m} \overset{kr\to 0}{\propto} \frac{\sqrt{\pi}}{\Gamma(|m|+1)}\left(\frac{kr}{2}\right)^{(1/2)+|m|}\cos\delta_m + \frac{\Gamma(|m|)}{\sqrt{\pi}}\left(\frac{kr}{2}\right)^{(1/2)-|m|}\sin\delta_m \tag{7}$$

for $|m|>0$, while for $m=0$ we have

$$u^{(k)}_{\mathrm{reg},0} \overset{kr\to 0}{\propto} \sqrt{\pi\frac{kr}{2}}\cos\delta_0 - \sqrt{\pi\frac{kr}{2}}\left[\ln\left(\frac{kr}{2}\right) + \gamma_E\right]\sin\delta_0. \tag{8}$$

At threshold $k=0$, two linearly independent solutions of the free equation ($U\equiv 0$) are $r^{(1/2)+|m|}$ and $r^{(1/2)-|m|}$ for $|m|>0$, and $\sqrt{r}$ and $\sqrt{r}\ln r$ for $m=0$. In the limit $k\to 0$, the expressions (7) and (8) become proportional to a k-independent superposition of these linearly independent threshold solutions, only if the k dependence of $\cos\delta_m$ and $\sin\delta_m$ compensates the difference in the k dependence entering via the argument $(kr/2)$. For $|m|>0$ this is achieved, for potentials falling off faster than $1/r^{2|m|+2}$, if

$$\tan\delta_m \overset{k\to 0}{\sim} \frac{\pm\pi}{\Gamma(|m|)\Gamma(|m|+1)}\left(\frac{ka_m}{2}\right)^{2|m|}. \tag{9}$$

For $m=0$ we need

$$\cot\delta_0 \overset{k\to 0}{\sim} \frac{2}{\pi}\left[\ln\left(\frac{ka}{2}\right) + \gamma_E\right]. \tag{10}$$

The appropriately normalized zero-energy solution $u^{(0)}_{\mathrm{reg},m}$ of Eq. (2) thus behaves for large r as

$$u^{(0)}_{\mathrm{reg},m\neq 0}(r) \overset{r\to\infty}{\sim} \sqrt{r}\left[\left(\frac{r}{a_m}\right)^{|m|} \pm \left(\frac{r}{a_m}\right)^{-|m|}\right],$$

$$u^{(0)}_{\mathrm{reg},m=0}(r) \overset{r\to\infty}{\sim} -\sqrt{r}\ln\left(\frac{r}{a}\right). \tag{11}$$

To understand the restriction to potentials falling off faster than $1/r^{2|m|+2}$, consider a potential behaving asymptotically as

$$U(r) \overset{r\to\infty}{\sim} \pm\frac{\hbar^2}{2M}\frac{(\beta_\alpha)^{\alpha-2}}{r^\alpha}, \quad \alpha>2. \tag{12}$$

The threshold solution of Eq. (2) is, at large r, essentially a superposition of Bessel functions of order $\mu=2|m|/(\alpha-2)$ and argument $z=2(\beta_\alpha/r)^{(\alpha-2)/2}/(\alpha-2)$ [18]. For an attractive potential tail, two linearly independent solutions at large r are $\sqrt{r}J_\mu(z)$ together with $\sqrt{r}J_{-\mu}(z)$ (if μ is not an integer) or

with $\sqrt{r}Y_\mu(z)$ (if μ is an integer). For large r (small z), the leading contribution to a superposition of $\sqrt{r}J_\mu(z)$ and $\sqrt{r}J_{-\mu}(z)$ [or $\sqrt{r}Y_\mu(z)$] comes from $J_{-\mu}$ (or Y_μ) and is proportional to $r^{(1/2)+|m|}$. The next-to-leading term contains a further factor $(z/2)^2 \propto (\beta_\alpha/r)^{\alpha-2}$ and is thus proportional to $r^{(1/2)+|m|+2-\alpha}$; this contribution should have a weaker r dependence than the leading contribution from $\sqrt{r}J_\mu(z)$, which is proportional to $r^{(1/2)-|m|}$, cf. Eq. (11), so the reasoning above and the expressions (9) and (10) are only applicable for $\alpha-2>2|m|$. The same arguments hold for a repulsive potential tail; the Bessel functions J_μ and Y_μ are merely replaced by I_μ and K_μ.

The constants a_m in Eq. (9) and a in Eq. (10) define a characteristic scale for the leading near-threshold behavior of the partial-wave scattering phase shift δ_m and deserve to be called the respective partial-wave scattering length. This is, in particular, true for the s-wave scattering length a, even though the leading near-threshold behavior of δ_0 is logarithmic and very different from the behavior of the s-wave phase shift in three dimensions [19–21]. The definition of the s-wave scattering length via Eqs. (10) and (11) is as already formulated by Verhaar *et al.* [11]. It has the advantage that the right-hand side of Eq. (10) gathers *all* contributions of order k^0, and that further contributions are of genuinely higher order (meaning not only through logarithmic factors) in k. For scattering by a hard circle of radius R_c, we have $\cot\delta_0 = Y_0(kR_c)/J_0(kR_c)$ and $a=R_c$ [8]. Alternative definitions of the s-wave scattering length have been proposed [22], but these generally lead to an additional and unnecessary term of order k^0, which is not helpful in practical calculations. The scattering length defined above resembles the s-wave scattering length in three dimensions in that it is the uniquely defined nontrivial zero of the threshold solution $v^{(0)}$ of the free equation with the same asymptotic behavior (11) as the threshold solution of Eq. (2). In three dimensions $v^{(0)}(r) \propto 1-r/a$, while in two dimensions $v^{(0)}(r) = -\sqrt{r}\ln(r/a)$. Note that, in two dimensions, a is well defined for any potential falling off faster than $1/r^2$ asymptotically, and a is always positive.

The logarithmic dependence on the wave number of the right-hand side of Eq. (10) is characteristic of s waves in two dimensions, so characteristic that it is worth introducing the logarithmic function

$$L(x) \stackrel{\text{def}}{=} \ln\left(\frac{x}{2}\right) + \gamma_E \tag{13}$$

as a special notation. The near-threshold behavior of quantities such as the s-wave phase shift are dominated by the logarithmic term, because the logarithm diverges for vanishing argument, $L(x) \stackrel{x\to 0}{\to} -\infty$. Positive powers x^p of x are of higher order than $L(x)$ for $x\to 0$. For a given positive argument x_0, however, $L(x_0)$ is zero, so x^p is no longer small compared to $L(x)$. The dimensionless number x_0 represents a natural upper limit for the dominance of the leading logarithmic term(s). Explicitly,

$$x_0 = 2e^{-\gamma_E} \approx 1.122\,919\,0, \quad L(x_0) = 0. \tag{14}$$

The amplitude $f(\theta)$ for scattering in two dimensions has the physical dimension of the square root of a length, and its partial-wave decomposition is

$$f(\theta) = \sum_{m=-\infty}^{+\infty} f_m e^{im\theta}, \quad f_m = \frac{1}{\sqrt{2i\pi k}}(S_m - 1), \tag{15}$$

where $S_m = e^{2i\delta_m}$ is the S matrix in the partial wave m. The differential scattering cross section $d\Lambda/d\theta$ and the total (elastic) scattering cross section Λ are lengths given by

$$\frac{d\Lambda}{d\theta} = |f(\theta)|^2 = \sum_{m,m'} f_m^* f_{m'} e^{i(m'-m)\theta},$$

$$\Lambda = \int_0^{2\pi} \frac{d\Lambda}{d\theta} d\theta = 2\pi \sum_{m=-\infty}^{+\infty} |f_m|^2 = \frac{4}{k}\sum_{m=-\infty}^{+\infty} \sin^2\delta_m. \tag{16}$$

Near threshold, both differential and total cross section are dominated by the s wave and diverge almost as $1/k$, "almost" meaning except for a logarithmic factor.

$$\frac{d\Lambda}{d\theta} \stackrel{k\to 0}{\sim} |f_0|^2, \quad \Lambda \stackrel{k\to 0}{\sim} 2\pi|f_0|^2 = \frac{4}{k}\sin^2\delta_0 = \frac{4/k}{1+\cot^2\delta_0}. \tag{17}$$

The next-to-leading contributions to the differential cross section are of order k^1; they come from the $|m|=1$ contribution to the scattering amplitude and from the next-to-leading contribution to the s-wave scattering phase shift, which we obtain via an effective-range expansion. Following the procedure familiar from three-dimensional scattering theory [19–21], we start with appropriately normalized regular solutions $u^{(k)}_{\text{reg},m=0}$ of Eq. (2), which behave asymptotically as

$$u^{(k)}_{\text{reg}}(r) \stackrel{r\to\infty}{\sim} \frac{\pi}{2}\sqrt{r}[J_0(kr)\cot\delta(k) - Y_0(kr)], \tag{18}$$

and the corresponding solutions $v^{(k)}$ of the free equation, which have the same asymptotic behavior,

$$v^{(k)}(r) = \frac{\pi}{2}\sqrt{r}[J_0(kr)\cot\delta(k) - Y_0(kr)]. \tag{19}$$

We drop the subscript 0 on the wave functions u,v and on the phase shift δ as long as we are obviously referring to s waves. From the Schrödinger equation (2) for $m=0$, taken at threshold and at finite wave number k, with and without the potential U we obtain

$$[u^{(0)}_{\text{reg}} u^{(k)\prime}_{\text{reg}} - u^{(0)\prime}_{\text{reg}} u^{(k)}_{\text{reg}} - (v^{(0)}v^{(k)\prime} - v^{(0)\prime}v^{(k)})]_0^\infty = k^2 I(k), \tag{20}$$

with

$$I(k) = \int_0^\infty [v^{(0)}(r)v^{(k)}(r) - u^{(0)}_{\text{reg}}(r)u^{(k)}_{\text{reg}}(r)]dr. \tag{21}$$

On the left-hand side of Eq. (20), the contributions from $r\to\infty$ vanish, because the solutions u with and v without potential obey the same boundary conditions. For $r\to 0$ the contribution from the u's, the regular solutions of Eq. (2),

vanish because of their boundary conditions, while the contribution from the v's (19) is

$$v^{(0)}v^{(k)\prime} - v^{(0)\prime}v^{(k)} \overset{r\to 0}{\sim} \frac{\pi}{2}\cot\delta - L(ka), \tag{22}$$

with the logarithmic function L as defined in Eq. (13) above. The leading behavior of $\cot\delta$ up to and including terms of order $O(k^2)$ thus is

$$\cot\delta \overset{k\to 0}{\sim} \frac{2}{\pi}\left[L(ka) + \frac{(kr_{\mathrm{eff}})^2}{2}\right], \tag{23}$$

with an "effective-range term" defined by

$$r_{\mathrm{eff}}^2 = 2\lim_{k\to 0} I(k) = 2\int_0^\infty [(v^{(0)}(r))^2 - (u_{\mathrm{reg}}^{(0)}(r))^2]dr, \tag{24}$$

as already formulated by Verhaar *et al.* [11]. Note that r_{eff}^2 can be negative.

In order to appreciate the range of applicability of the effective-range expansion (23), consider again a potential behaving asymptotically as Eq. (12). The zero-energy solutions $u_{\mathrm{reg}}^{(0)}$ of Eq. (2) for $m=0$ then behave asymptotically as a superposition of Bessel functions of order zero and argument $z=2(\beta_\alpha/r)^{(\alpha-2)/2}/(\alpha-2)$. The leading contribution for large r (small z) is a term identical to $v^{(0)}=-\sqrt{r}\ln(r/a)$, and the next-to-leading contribution contains a further factor proportional to z^2, i.e., to $r^{-(\alpha-2)}$. The leading contribution to $(v^{(0)})^2-(u_{\mathrm{reg}}^{(0)})^2$ is thus proportional to $r^{(3-\alpha)}\ln(r/a)^2$, so the integral on the right-hand side of Eq. (24) converges to a well-defined limit for $\alpha>4$.

III. QUANTUM REFLECTION

For deep potentials with attractive tails falling off more rapidly than $-1/r^2$, as typically occur in the interaction of atoms or molecules with a conducting or dielectric surface, the motion of the projectile becomes classical not only at large distances, but also for "small" distances. Here "small" refers to a comparison with typical length scales of the potential tail, which may be many hundreds or thousands of atomic units [23]. In the close region of a few atomic units or so, the interaction depends more significantly on the internal microscopic structure of target and projectile and is usually quite complicated. When the short-ranged part of the interaction leads to inelastic reactions so efficiently that we can assume total absorption from the elastic channel in the close region, then the yield of elastically scattered particles is entirely due to quantum reflection, i.e., to classically forbidden reflection in the absence of a classical turning point. Quantum reflection occurs in the distant, nonclassical region of the attractive potential tail in the scattering of atoms from conducting or dielectric flat surfaces [12,13,24–29], and in s-wave scattering of atoms from a sphere [14]. For scattering in two dimensions, the s-wave centrifugal potential is purely attractive. When it is supplemented by an attractive potential tail more singular than $-1/r^2$, motion becomes classical and the WKB approximation becomes increasingly accurate at small distances just as in the one-dimensional (flat surface) and three-dimensional cases, so the quantum reflection amplitude can be defined uniquely via incoming boundary conditions for small r—this is an unambiguous representation of complete absorption in the close regime.

In order to determine the amplitude for s-wave quantum reflection in two dimensions, we study complex solutions $\mathfrak{u}^{(k)}(r)$ of the radial Schrödinger equation (with the real potential U_{tail}), which obey incoming boundary conditions at small r and behave asymptotically (large r) as

$$\mathfrak{u}^{(k)}(r) \sim \frac{\pi}{2}\sqrt{r}[J_0(kr)\cot\mathfrak{d} - Y_0(kr)] \overset{r\to\infty}{\propto} e^{-ikr} + R(k)e^{+ikr}. \tag{25}$$

This has the same form as already given in Eqs. (6) and (18), except that the phase shift $\mathfrak{d}$ is now complex and the S matrix $S_{m=0}=iR=\exp(2i\mathfrak{d})$ is no longer necessarily unitary, $|S_0|=|R|\leqslant 1$. The complex phase shift $\mathfrak{d}$ is related to the quantum reflection amplitude R by

$$i\cot\mathfrak{d} = \frac{1+iR}{1-iR}, \quad R = -i\exp(2i\mathfrak{d}) = -i\frac{\cot\mathfrak{d}+i}{\cot\mathfrak{d}-i}. \tag{26}$$

At threshold, the complex wave function (25) assumes a k-independent form, $\mathfrak{u}^{(0)}(r) \overset{r\to\infty}{\sim} -\sqrt{r}\ln(r/\mathfrak{a})$ characterized by a (complex) scattering length $\mathfrak{a}$. As in Sec. II, an effective-range theory based on the wave functions (25) and the corresponding solutions of the free equation,

$$\mathfrak{v}^{(k)}(r) = \frac{\pi}{2}\sqrt{r}[J_0(kr)\cot\mathfrak{d} - Y_0(kr)],$$

$$\mathfrak{v}^{(0)}(r) = -\sqrt{r}\ln\left(\frac{r}{\mathfrak{a}}\right) = -\sqrt{r}\ln\left(\frac{r}{|\mathfrak{a}|}\right) + i\arg(\mathfrak{a})\sqrt{r}, \tag{27}$$

yields an effective-range expansion of the cotangent of the complex phase shift $\mathfrak{d}$,

$$\cot\mathfrak{d} \overset{k\to 0}{\sim} \frac{2}{\pi}\left[\ln\left(\frac{k\mathfrak{a}}{2}\right) + \gamma_{\mathrm{E}} + \frac{1}{2}(k\mathfrak{r}_{\mathrm{eff}})^2\right], \tag{28}$$

with the complex effective range defined by

$$\mathfrak{r}_{\mathrm{eff}}^2 = 2\int_0^\infty [(\mathfrak{v}^{(0)}(r))^2 - (\mathfrak{u}^{(0)}(r))^2]dr. \tag{29}$$

Here $\mathfrak{u}^{(0)}(r)$ is the threshold solution of the Schrödinger equation (including the singular attractive potential), which behaves asymptotically as $\mathfrak{v}^{(0)}(r)$ given in Eq. (27).

The complex scattering length $\mathfrak{a}$ can be related to the amplitudes and phases of two linearly independent real threshold solutions,

$$u^{(0)}(r) \overset{r\to\infty}{\sim} \sqrt{r}, \quad w_\lambda^{(0)}(r) \overset{r\to\infty}{\sim} -\sqrt{r}\ln\left(\frac{r}{\lambda}\right), \tag{30}$$

where λ is a length, yet to be determined, which ensures that the argument of the logarithm is dimensionless. At small distances, where the WKB approximation is accurate, both $u^{(0)}$ and $w_\lambda^{(0)}$ can be written as WKB waves with real amplitudes D_0, B_0,

$$u^{(0)}(r) = \frac{D_0}{\sqrt{p_0(r)}} \cos[I^{(0)}_{\text{tail}}(r)], \quad w^{(0)}_{\lambda}(r) = \frac{B_0}{\sqrt{p_0(r)}} \cos[I^{(0)}_{\text{tail}}(r)]. \tag{31}$$

Here $I^{(0)}_{\text{tail}}(r)$ is essentially the action integral involving the local classical momentum at threshold, $p_0 = \sqrt{\hbar^2/(4r^2) - 2MU_{\text{tail}}(r)}$,

$$I^{(0)}_{\text{tail}}(r) = \frac{1}{\hbar}\int_r^{r_O} p_0(r')dr' - \Phi(r_O). \tag{32}$$

The integral can only be taken to a finite upper limit r_O without diverging, and it is regularized by subtracting a phase $\Phi(r_O)$, which diverges in the same way for $r_O \to \infty$. For sufficiently large r_O, $I^{(0)}_{\text{tail}}(r)$ must be independent of r_O, and its phase is defined such that the WKB representation (31) of $u^{(0)}(r)$ agrees with the exact wave function for $r \to 0$. The integrand $J^{(0)}_{\text{tail}}(r)$ describing the r dependence of $w^{(0)}_{\lambda}$ in the WKB region differs from $I^{(0)}_{\text{tail}}(r)$ by an r-independent phase which depends on the length λ governing the relative weights of the $\sqrt{r}$ and the $\sqrt{r}\ln(r)$ contributions in $w^{(0)}_{\lambda}$. A simple possibility of defining the length λ is to require $w^{(0)}_{\lambda}(r)$ to be phase shifted for $r \to 0$ by $\frac{\pi}{2}$ relative to the uniquely defined wave function $u^{(0)}(r)$, which tends to $\sqrt{r}$ asymptotically,

$$J^{(0)}_{\text{tail}}(r) \overset{r\to 0}{\sim} I^{(0)}_{\text{tail}}(r) - \frac{\pi}{2} \Rightarrow w^{(0)}_{\lambda}(r) \overset{r\to 0}{\sim} \frac{B_0}{\sqrt{p_0(r)}} \sin[I^{(0)}_{\text{tail}}(r)]. \tag{33}$$

The linear combination of $u^{(0)}$ and $w^{(0)}_{\lambda}$, which describes incoming boundary conditions for $r \to 0$, is thus

$$\mathfrak{u}^{(0)}(r) \propto u^{(0)}(r) + i\frac{D_0}{B_0} w^{(0)}_{\lambda}(r) \overset{r\to 0}{\sim} \frac{D_0}{\sqrt{p_0(r)}} \exp\left[\frac{i}{\hbar}\int_r^{r_O} p(r')dr' - \Phi(r_O)\right]. \tag{34}$$

Inspection of the asymptotic ($r \to \infty$) behavior (27) of $\mathfrak{u}^{(0)}(r)$ shows

$$\lambda = |\mathfrak{a}|, \quad \arg(\mathfrak{a}) = -\frac{B_0}{D_0}. \tag{35}$$

With the definition (13) of the real logarithmic function L, Eq. (28) can be written as

$$\cot\mathfrak{d} \overset{k\to 0}{\sim} \frac{2}{\pi}\left[L(k|\mathfrak{a}|) + \frac{k^2}{2}\,\text{Re}[\mathfrak{r}^2_{\text{eff}}] + i\left(\arg(\mathfrak{a}) + \frac{k^2}{2}\,\text{Im}[\mathfrak{r}^2_{\text{eff}}]\right)\right]. \tag{36}$$

Inserting this into the expression (26) for R gives

$$R \overset{k\to 0}{\sim} -i\left[1 + \frac{i\pi}{L(k|\mathfrak{a}|) + \frac{1}{2}k^2\,\text{Re}[\mathfrak{r}^2_{\text{eff}}] + i\left\{\arg(\mathfrak{a}) - \frac{\pi}{2} + \frac{1}{2}k^2\,\text{Im}[\mathfrak{r}^2_{\text{eff}}]\right\}}\right]. \tag{37}$$

IV. NEAR-THRESHOLD QUANTIZATION

A potential well with a tail falling off faster than $1/r^2$ can support (at most) a finite number of bound states. This also holds for s waves in two dimensions, even though the radial Schrödinger equation (2) contains an attractive centrifugal term $-\frac{1}{4}\hbar^2/(2Mr^2)$ [30]. The bound-state energies E_n are determined by a quantization function $F(E)$ according to the quantization rule

$$n_{\text{th}} - n = F(E_n), \tag{38}$$

where n_{th} is the not necessarily integer threshold quantum number. An integer value of n_{th} implies the existence of a bound state exactly at threshold. For s waves in three dimensions we have recently demonstrated [15,16] how knowledge of the near-threshold behavior of $F(E)$ can be used to immediately read off scattering lengths from the energy of a high-lying (not necessarily the highest-lying) bound state, or to determine to very high accuracy the dissociation limit from spectroscopic energies of high-lying states. In this section we adapt the subthreshold effective-range theory described in [16] in order to derive the leading contributions to the near-threshold behavior of $F(E)$ for s waves in the two-dimensional case.

The potential $U(r)$ is, for large distances, described by the attractive tail $U_{\text{tail}}(r)$, which is more singular than $-1/r^2$. The WKB approximation of the Schrödinger equation (2) with U_{tail} becomes increasingly accurate for small r. We assume that the region where the WKB approximation is sufficiently accurate overlaps with the region in coordinate space where the full potential $U(r)$ is well represented by U_{tail}. The solution of the radial Schrödinger equation (2) (with $m=0$), which obeys decaying boundary conditions for large r is

$$u_{\kappa}(r) \overset{r\to\infty}{\sim} \exp(-\kappa r). \tag{39}$$

In the WKB region, u_{κ} can be written as a WKB wave,

$$u_{\kappa}(r) = \frac{\mathcal{D}(\kappa)}{\sqrt{p_{\kappa}(r)}} \cos\left(\frac{1}{\hbar}\int_r^{r_{\text{out}}(E)} p_{\kappa}(r')dr' - \frac{\phi_{\text{out}}(E)}{2}\right). \tag{40}$$

Here $r_{\text{out}}(E)$ is the outer classical turning point and $\phi_{\text{out}}(E)$ is the outer reflection phase, which is defined such that the

wave function on the right-hand side of Eq. (40) has the correct phase in the WKB region. Coming from short distances we have,

$$u_\kappa(r) \propto \frac{1}{\sqrt{p_\kappa(r)}} \cos\left(\frac{1}{\hbar}\int_{r_{\rm in}(E)}^{r} p_\kappa(r')dr' - \frac{\phi_{\rm in}(E)}{2}\right), \quad (41)$$

where $\phi_{\rm in}(E)$ is the reflection phase at the inner classical turning point $r_{\rm in}(E)$. Bound states exist at energies E_n for which the two wave functions (40) and (41) match, which leads to the generalized WKB quantization rule [23],

$$\frac{1}{\hbar}S(E_n) \equiv \frac{1}{\hbar}\int_{r_{\rm in}(E_n)}^{r_{\rm out}(E_n)} p_\kappa(r)dr = n\pi + \frac{\phi_{\rm in}(E_n)}{2} + \frac{\phi_{\rm out}(E_n)}{2}. \quad (42)$$

The only condition for the applicability of Eq. (42) is, that there is a WKB region (which can be arbitrarily small) between the inner and outer classical turning points, where the WKB approximation is accurate. Subtracting Eq. (42) from its threshold version ($E=0$) leads to the quantization rule (38) with the quantization function

$$F(E) \equiv \frac{S(0)}{\pi\hbar} - \frac{\phi_{\rm out}(0)}{2\pi} - \left(\frac{S(E)}{\pi\hbar} - \frac{\phi_{\rm out}(E)}{2\pi}\right) - \frac{\phi_{\rm in}(0) - \phi_{\rm in}(E)}{2\pi}. \quad (43)$$

The expression (43) is a bit more subtle than the corresponding expression for the quantization function for s waves in three dimensions [16], because, due to the attractive centrifugal term in the Schrödinger equation, the action integral $S(E)$ diverges in the limit $E\to 0$. However, the outer reflection phase $\phi_{\rm out}$ also diverges, and the difference $\frac{1}{\hbar}S(E)-\frac{1}{2}\phi_{\rm out}(E)$ assumes a well-defined value in this limit, which we write as $\frac{1}{\hbar}S(0)-\frac{1}{2}\phi_{\rm out}(0)$ for transparency.

The contribution of the potential tail to the quantization function (43) can be written as

$$F_{\rm tail}(E) \equiv \frac{S_{\rm tail}(0)}{\pi\hbar} - \frac{\phi_{\rm out}(0)}{2\pi} - \left(\frac{S_{\rm tail}(E)}{\pi\hbar} - \frac{\phi_{\rm out}(E)}{2\pi}\right), \quad (44)$$

where all quantities are now defined for the potential $U_{\rm tail}$, e.g.,

$$S_{\rm tail}(E) = \int_{r_l}^{r_{\rm out}(E)} p_\kappa(r')dr',$$

$$p_\kappa(r) = \sqrt{\hbar^2/(4r^2) + 2M[E - U_{\rm tail}(r)]}. \quad (45)$$

The lower integration limit r_l in Eq. (45) can be arbitrarily small. Although the small-distance contributions to the action integrals diverge for $r_l\to 0$, their difference remains finite in this limit. The error caused by neglecting the contribution from the inner reflection phases in Eq. (44) and by replacing the action integrals from the full potential with $S_{\rm tail}$ depends smoothly and analytically on E, and it vanishes at threshold, so we can write

$$F(E) = F_{\rm tail}(E) + F_{\rm sr}(E), \quad F_{\rm sr}(E) \overset{E\to 0}{\sim} \gamma_{\rm sr}E + O(E^2). \quad (46)$$

Here $F_{\rm sr}$ is the contribution from the short-ranged part of the potential and $\gamma_{\rm sr}$ is the coefficient in its leading term.

Guided by the procedure used in Secs. II and III to derive the effective-range expansion of scattering theory or quantum reflection above threshold, or in Ref. [16] for the quantization function for s waves in three dimensions, we consider the wave function u_κ, which solves the radial Schrödinger equation (2)—with $m=0$ and the potential $U_{\rm tail}$—at energy $E=-\hbar^2\kappa^2/(2M)$, and the solution v_κ of the free equation (without $U_{\rm tail}$) obeying the same boundary conditions,

$$v_\kappa(r) = i\sqrt{\frac{\pi\kappa r}{2}}H_0^{(1)}(i\kappa r) \overset{r\to\infty}{\sim} e^{-\kappa r},$$

$$u_\kappa(r) \overset{r\to\infty}{\sim} v_\kappa(r). \quad (47)$$

Here $H_0^{(1)}=J_0+iY_0$ is the Hankel function [17].

Again, taking the limit $\kappa\to 0$ is a bit more subtle than for s waves in three dimensions. Since

$$H_0^{(1)}(i\kappa r) \overset{\kappa r\to 0}{\sim} \frac{2i}{\pi}L(\kappa r), \quad (48)$$

with the logarithmic function L as defined in Eq. (13), we need to renormalize the wave functions (47) in order to get κ-independent limits at threshold. To this end we again introduce a length λ, to be determined, and we divide the wave functions (47) by $-\sqrt{\frac{2}{\pi}}\kappa L(\kappa\lambda)$,

$$v_\lambda^{(\kappa)}(r) = \frac{\pi}{2i}\sqrt{r}\frac{H_0^{(1)}(i\kappa r)}{L(\kappa\lambda)} \overset{\kappa\to 0}{\sim} \sqrt{r},$$

$$u_\lambda^{(\kappa)}(r) \overset{r\to\infty}{\sim} v_\lambda^{(\kappa)}(r), \quad u_\lambda^{(\kappa)}(r) \overset{\kappa\to\infty}{\to} u^{(0)}(r) \overset{r\to\infty}{\sim} \sqrt{r}. \quad (49)$$

From the Schrödinger equation (2), with the potential $U_{\rm tail}$, we obtain

$$\int_{r_l}^{r_u}(u^{(0)}u_\lambda^{(\kappa)\prime\prime} - u^{(0)\prime\prime}u_\lambda^{(\kappa)})dr = [u^{(0)}u_\lambda^{(\kappa)\prime} - u^{(0)\prime}u_\lambda^{(\kappa)}]_{r_l}^{r_u} = \kappa^2\int_{r_l}^{r_u} u^{(0)}u_\lambda^{(\kappa)}dr \quad (50)$$

for arbitrary lower and upper integration limits r_l and r_u. The contribution from the upper integration limit to the right-hand side of the upper line of Eq. (50) vanishes in the limit $r_u\to\infty$, because $u_\lambda^{(\kappa)}\propto\exp(-\kappa r)$ and $u_\lambda^{(\kappa)\prime}\propto-\kappa\exp(-\kappa r)$. We obtain the contribution from the lower integration limit r_l by looking at the wave functions $u_\lambda^{(\kappa)}$ [cf. Eq. (40)] and their derivatives,

$$u_\lambda^{(\kappa)\prime}(r)=\frac{\mathcal{D}_\lambda(\kappa)}{\sqrt{p_\kappa(r)}}\left[-\frac{1}{2}\frac{p_\kappa'(r)}{p_\kappa(r)}\cos\left(\frac{1}{\hbar}\int_r^{r_E}p_\kappa(r')dr'-\frac{\phi_{\text{out}}(E)}{2}\right)+\frac{p_\kappa(r)}{\hbar}\sin\left(\frac{1}{\hbar}\int_r^{r_E}p_\kappa(r')dr'-\frac{\phi_{\text{out}}(E)}{2}\right)\right],\tag{51}$$

where $\mathcal{D}_\lambda(\kappa)=-\sqrt{\pi/(2\kappa)}\mathcal{D}(\kappa)/L(\kappa\lambda)$. Since U_{tail} is more singular than $-1/r^2$ for small r, $1/p_\kappa(r)$ vanishes more rapidly than r and the contributions from the cosine term in Eq. (51) to products such as $u^{(0)}u_\lambda^{(\kappa)\prime}$ in Eq. (50) vanish for $r_l\to 0$. Introducing the abbreviation

$$I_{\text{tail}}^{(\kappa)}=\frac{S_{\text{tail}}(E)}{\hbar}-\frac{\phi_{\text{out}}(E)}{2},\tag{52}$$

we obtain from Eqs. (40) and (51),

$$[u^{(0)}u_\lambda^{(\kappa)\prime}-u^{(0)\prime}u_\lambda^{(\kappa)}]_{r_l\to 0}=\frac{\mathcal{D}_\lambda(\kappa)\mathcal{D}_\lambda(0)}{\hbar}\sin(I_{\text{tail}}^{(\kappa)}-I_{\text{tail}}^{(0)}).\tag{53}$$

Equation (52) extends the definition (32) in Sec. III to subthreshold energies. The integrals diverge as $r_l\to 0$, but the difference $I_{\text{tail}}^{(\kappa)}-I_{\text{tail}}^{(0)}$ remains well defined.

From the free Schrödinger equation without potential we have

$$[\sqrt{r}v_\lambda^{(\kappa)\prime}-(\sqrt{r})'v_\lambda^{(\kappa)}]_{r_l}^{r_u}=\kappa^2\int_{r_l}^{r_u}\sqrt{r}v_\lambda^{(\kappa)}dr.\tag{54}$$

Again, the contributions from r_u vanish for $r_u\to\infty$, while the contributions from r_l are

$$[\sqrt{r}v_\lambda^{(\kappa)\prime}-(\sqrt{r})'v_\lambda^{(\kappa)}]_{r_l\to 0}=\frac{1}{L(\kappa\lambda)}.\tag{55}$$

Combining Eqs. (50) and (53)–(55) gives

$$\frac{\mathcal{D}_\lambda(0)\mathcal{D}_\lambda(\kappa)}{\hbar}\sin(I_{\text{tail}}^{(0)}-I_{\text{tail}}^{(\kappa)})=-\frac{1}{L(\kappa)}-\kappa^2\int_0^\infty[\sqrt{r}v_\lambda^{(\kappa)}(r)-u^{(0)}(r)u_\lambda^{(\kappa)}(r)]dr.\tag{56}$$

Inverting this expression provides an exact expression for the tail contribution (44) to the quantization function,

$$\pi F_{\text{tail}}(E)=\frac{S_{\text{tail}}(0)}{\hbar}-\frac{\phi_{\text{out}}(0)}{2}-\left(\frac{S_{\text{tail}}(E)}{\hbar}-\frac{\phi_{\text{out}}(E)}{2}\right)=\arcsin\left[\frac{\hbar}{\mathcal{D}_\lambda(0)\mathcal{D}_\lambda(\kappa)}\left(-\frac{1}{L(\kappa\lambda)}-\frac{\kappa^2\rho^2}{2}\right)\right],\tag{57}$$

where ρ^2 has the dimension of a length squared and is given by

$$\rho^2(E)=2\int_0^{+\infty}[\sqrt{r}v_\lambda^{(\kappa)}(r)-u^{(0)}(r)u_\lambda^{(\kappa)}(r)]dr.\tag{58}$$

The near-threshold behavior of F_{tail} is determined by the near-threshold behavior of $\mathcal{D}_\lambda(\kappa)$, and the subthreshold effective range ρ_{eff} given by the threshold limit of Eq. (58),

$$\rho_{\text{eff}}^2=2\int_0^\infty[r-(u^{(0)}(r))^2]dr.\tag{59}$$

In order to understand the near-threshold behavior of $\mathcal{D}_\lambda(\kappa)$ we study the threshold solution $u^{(0)}$, which behaves asymptotically as $u^{(0)}(r)\overset{r\to\infty}{\sim}\sqrt{r}$ [cf. Eq. (49)], and a linearly independent second solution $w_\lambda^{(0)}$ of the Schrödinger equation (with U_{tail}), which behaves asymptotically as

$$w_\lambda^{(0)}(r)\overset{r\to\infty}{\sim}-\sqrt{r}\ln\left(\frac{r}{\lambda}\right).\tag{60}$$

As in Sec. III we now choose the length λ to be equal to the modulus $|\mathfrak{a}|$ of the complex scattering length $\mathfrak{a}$ defining the leading near-threshold behavior of the amplitude for quantum reflection by U_{tail} [see Eqs. (26), (28), and (35)]. Since the energy enters the Schrödinger equation linearly, we can express the near-threshold behavior of the asymptotically decaying solution $u_{\lambda=|\mathfrak{a}|}^{(\kappa)}$, to order below κ^2, as a superposition of the linearly independent threshold solutions $u^{(0)}$ and $w_{\lambda=|\mathfrak{a}|}^{(0)}$ with κ-dependent coefficients. From the asymptotic behavior (49) of $u_{\lambda=|\mathfrak{a}|}^{(\kappa)}$ and the near-threshold behavior (48) of $H_0^{(1)}$ we see that the correct superposition is

$$u_{\lambda=|\mathfrak{a}|}^{(\kappa)}(r)=u^{(0)}(r)-\frac{w_{\lambda=|\mathfrak{a}|}^{(0)}(r)}{L(\kappa|\mathfrak{a}|)}+O(\kappa^2).\tag{61}$$

In the WKB region we can exploit Eqs. (31) and (33) to write

$$u_{\lambda=|\mathfrak{a}|}^{(\kappa)}(r)=\frac{D_0}{\sqrt{p_0(r)}}[\cos(I_{\text{tail}}^{(0)}(r))+A(\kappa)\sin(I_{\text{tail}}^{(0)}(r))]+O(\kappa^2)=\frac{D_0\sqrt{1+A(\kappa)^2}}{\sqrt{p_0(r)}}\cos[I_{\text{tail}}^{(0)}(r)-\arctan(A(\kappa))]+O(\kappa^2),\tag{62}$$

with the abbreviation

$$A(\kappa)=-\frac{B_0}{D_0L(\kappa|\mathfrak{a}|)}.\tag{63}$$

An alternative expression for $u_{\lambda=|\mathfrak{a}|}^{(\kappa)}$ is provided by Eq. (40)—divided by $-\sqrt{\frac{2}{\pi}}\kappa L(\kappa|\mathfrak{a}|)$. Comparing the amplitude in Eq. (62) with the alternative expression (40) gives

$$\mathcal{D}_{\lambda=|\mathfrak{a}|}(\kappa)\overset{\kappa\to 0}{\sim}D_0\left[\sqrt{1+A(\kappa)^2}+\frac{(\kappa d)^2}{2}\right],\quad \mathcal{D}_{\lambda=|\mathfrak{a}|}(0)=D_0.\tag{64}$$

We expect a term of order κ^2 due to the contributions $O(\kappa^2)$ on the right-hand sides of Eqs. (61) and (62); d is some length characterizing this term.

Comparing the phase in Eq. (62) with the alternative expression (40) gives

$$\frac{1}{\hbar}\int_{r}^{r_{\mathrm{out}}(E)} p_\kappa(r')dr' - \frac{\phi_{\mathrm{out}}}{2} = I_{\mathrm{tail}}^{(E)}(r) \overset{\kappa\to 0}{\sim} I_{\mathrm{tail}}^{(0)}(r) - \arctan(A(\kappa)) + O(\kappa^2). \quad (65)$$

Comparing Eq. (65) with the leading contributions to Eq. (57) shows that $\hbar/D_0^2 = B_0/D_0 = -\arg(\mathfrak{a})$, so

$$A(\kappa) = \frac{\arg(\mathfrak{a})}{L(\kappa|\mathfrak{a}|)}. \quad (66)$$

Inserting these results into the subthreshold effective-range expansion (57) yields the following formula for the near-threshold behavior of the tail contribution F_{tail} to the quantization function,

$$\sin(\pi F_{\mathrm{tail}}(E)) \overset{\kappa\to 0}{\sim} \frac{A(\kappa)}{\sqrt{1+A(\kappa)^2}} \times\left(1 + L(\kappa|\mathfrak{a}|)\frac{(\kappa\rho_{\mathrm{eff}})^2}{2} - \frac{(\kappa d)^2/2}{\sqrt{1+A(\kappa)^2}}\right). \quad (67)$$

Up to and including terms of order κ^2 we thus have

$$\pi F_{\mathrm{tail}}(E) \overset{\kappa\to 0}{\sim} \arctan(A(\kappa)) + \arg(\mathfrak{a})\left[\frac{(\kappa\rho_{\mathrm{eff}})^2}{2} - \frac{(\kappa d)^2/2}{\sqrt{\arg(\mathfrak{a})^2 + L(\kappa|\mathfrak{a}|)^2}}\right]. \quad (68)$$

For the expansion of functions containing a logarithmic dependence on the argument, it is important to realize that any finite power of the logarithm does not significantly change the order of a term corresponding to a given power of the argument. Thus any power of $A(\kappa)$ in the Taylor series for $\arctan(A(\kappa))$ in Eq. (68) is essentially of order κ^0. Among the terms of order κ^2, the contribution proportional to ρ_{eff}^2 is the leading one, but the next term containing the less readily accessible parameter d is smaller only by the reciprocal of a logarithm.

V. SCATTERING LENGTHS AND NEAR-THRESHOLD QUANTIZATION

The real scattering length a introduced in Sec. II, see Eq. (11), depends on the whole potential U and not only on the (singular) potential tail U_{tail}. The same is true for the threshold quantum number n_{th} which, together with the quantization function, determines the bound state energies. Both are connected through a relation containing parameters of U_{tail} as only further ingredients. To derive this relation we look at the two wave functions $u^{(0)}$ and $w_\lambda^{(0)}$, which solve the radial Schrödinger equation (2) (for $m=0$) with the potential U_{tail} and behave asymptotically as $\sqrt{r}$ and $-\sqrt{r}\ln(r/\lambda)$, respectively, [see Eqs. (49) and (60)], and we again assume that the parameter λ is the modulus of the complex scattering length $\mathfrak{a}$, which determines the leading near-threshold behavior of the quantum reflection amplitude as described in Sec. III and is a property only of the potential tail. The regular threshold solution $u_{\mathrm{reg}}^{(0)}$ of the Schrödinger equation, with the full potential U, behaves asymptotically as

$$u_{\mathrm{reg}}^{(0)}(r) \overset{r\to\infty}{\propto} -\sqrt{r}\ln\left(\frac{r}{a}\right) = -\sqrt{r}\left[\ln\left(\frac{r}{|\mathfrak{a}|}\right) - \ln\left(\frac{a}{|\mathfrak{a}|}\right)\right]. \quad (69)$$

At distances where the full potential U is well represented by U_{tail} it is a superposition of the solutions $u^{(0)}(r)$ and $w_{\lambda=|\mathfrak{a}|}^{(0)}(r)$,

$$u_{\mathrm{reg}}^{(0)}(r) = w_{\lambda=|\mathfrak{a}|}^{(0)}(r) + \ln\left(\frac{a}{|\mathfrak{a}|}\right)u^{(0)}(r). \quad (70)$$

In the WKB region we can exploit Eqs. (31) and (33) to write

$$u_{\mathrm{reg}}^{(0)}(r) \propto \frac{B_0}{\sqrt{p_0(r)}}\left[\sin(I_{\mathrm{tail}}^{(0)}(r)) + \frac{D_0}{B_0}\ln\left(\frac{a}{|\mathfrak{a}|}\right)\cos(I_{\mathrm{tail}}^{(0)}(r))\right] \propto \frac{1}{\sqrt{p_0(r)}}\cos(I_{\mathrm{tail}}^{(0)}(r) - \eta), \quad \cot\eta = \frac{D_0}{B_0}\ln\left(\frac{a}{|\mathfrak{a}|}\right). \quad (71)$$

We can also write $u_{\mathrm{reg}}^{(0)}$ as a WKB wave with reference to the inner classical turning point $r_{\mathrm{in}}(0)$ of the full potential,

$$u_{\mathrm{reg}}^{(0)}(r) \propto \frac{1}{\sqrt{p_0(r)}}\cos\left(\frac{1}{\hbar}\int_{r_{\mathrm{in}}(0)}^{r} p_0(r')dr' - \frac{\phi_{\mathrm{in}}}{2}\right). \quad (72)$$

The argument of the cosine in Eq. (72) must agree to within a sign and/or an integral multiple of π with that in the lower line of Eq. (71), giving the following condition which no longer depends on the exact value of r, as long as r lies in the WKB region:

$$\frac{1}{\hbar}\int_{r_{\mathrm{in}}(0)}^{r} p_0(r')dr' - \frac{\phi_{\mathrm{in}}}{2} + I_{\mathrm{tail}}^{(0)}(r) = \eta - n\pi + O(\kappa^2). \quad (73)$$

This is, to order below κ^2, the threshold version of the quantization condition (42); the fact that $I_{\mathrm{tail}}^{(0)}(r)$ is defined with the potential U_{tail} according to Eq. (32) instead of with the full potential only affects the result in order κ^2. With Eq. (35), the relation connecting scattering length a with threshold quantum number n_{th} is

$$n_{\mathrm{th}} \overset{\mathrm{def}}{=} \frac{\eta}{\pi} = \frac{1}{\pi}\arctan\left(-\frac{\arg(\mathfrak{a})}{\ln(a/|\mathfrak{a}|)}\right),$$

$$a = |\mathfrak{a}|\exp\left(-\frac{\arg(\mathfrak{a})}{\tan(\pi n_{\mathrm{th}})}\right). \quad (74)$$

For a bound state exactly at threshold, n_{th} is the integer and a is undefined, as in the three-dimensional case. In contrast to the three-dimensional case, however, the scattering length (74) is always positive when defined, i.e., for noninteger n_{th}.

If there is a bound state at energy $E=-\hbar^2\kappa_n^2/(2M)$ very close to threshold, we can use the quantization rule (38) with

TABLE I. Characteristic parameters for homogeneous potentials. The first two rows show the (real) scattering length a^{rep} (80) for the repulsive potential (76) and the argument $\arg(\mathfrak{a})$ (87) of the complex scattering length $\mathfrak{a}$ for the attractive potential tail (85). Remember that $|\mathfrak{a}|=a^{\mathrm{rep}}$ according to Eq. (89). The third row shows the dimensionless number x_α, which gives the value of $k\beta_\alpha$ (or $\kappa\beta_\alpha$) at which the logarithmic function $L(k|\mathfrak{a}|)$ [or $L(\kappa|\mathfrak{a}|)$ vanishes, cf. Eq. (82)]. The next three rows show the effective range squared $(r_{\mathrm{eff}}^{\mathrm{rep}})^2$ (83) for the repulsive potential (76), and both real and imaginary parts of the complex effective range squared $\mathfrak{r}_{\mathrm{eff}}^2$ (90) for the attractive potential tail (85). The last row shows the subthreshold effective range squared ρ_{eff}^2 (99). All lengths are in units of β_α and all squared lengths are in units of β_α^2.

α	3	4	5	6	7	8	$\alpha\to\infty$
$a^{\mathrm{rep}}/\beta_\alpha$	3.1722190	0.8905362	0.7063830	0.6672841	0.6617358	0.6670782	1
$\arg(\mathfrak{a})/\pi$	−1	$-\frac{1}{2}$	$-\frac{1}{3}$	$-\frac{1}{4}$	$-\frac{1}{5}$	$-\frac{1}{6}$	$-\frac{1}{\alpha-2}$
x_α	0.3539853	1.2609470	1.5896745	1.6828198	1.6969295	1.6833392	1.1229190
$(r_{\mathrm{eff}}^{\mathrm{rep}})^2/\beta_\alpha^2$		see Eq. (119)	−1.4651483	0	0.1478103	0.1900491	$\frac{1}{2}$
$\mathrm{Re}[\mathfrak{r}_{\mathrm{eff}}^2]/\beta_\alpha^2$		see Eq. (115)	0.7325741	0	0.0456759	0.0950245	$\frac{1}{2}$
$\mathrm{Im}[\mathfrak{r}_{\mathrm{eff}}^2]/\beta_\alpha^2$		see Eq. (115)	1.2688556	0	−0.1405759	−0.1645873	$-\frac{\pi}{\alpha-2}$
$\rho_{\mathrm{eff}}^2/\beta_\alpha^2$			1.0020413	0.6366198	0.5479553	0.5199119	1

the expression (68) for the quantization function to express the scattering length (74) in terms of κ_n,

$$a \overset{\kappa_n\to 0}{\sim} \frac{2e^{-\gamma_{\mathrm{E}}}}{\kappa_n} + \kappa_n e^{-\gamma_{\mathrm{E}}}\rho_{\mathrm{eff}}^2[\arg(\mathfrak{a})^2 + L(\kappa_n|\mathfrak{a}|)^2] - \kappa_n e^{-\gamma_{\mathrm{E}}} d^2\sqrt{\arg(\mathfrak{a})^2 + L(\kappa_n|\mathfrak{a}|)^2}. \tag{75}$$

A possible contribution from short-range effects to the quantization function according to Eq. (46) is accounted for by replacing ρ_{eff}^2 with $\rho_{\mathrm{eff}}^2 - \gamma_{\mathrm{sr}}\hbar^2/(M\arg(\mathfrak{a}))$ on the right-hand side of Eq. (75). Note that, in contrast to the analogous expansion for s-wave scattering lengths in three dimensions [16], the right-hand side of Eq. (75) contains no contribution of order κ_n^0.

VI. APPLICATION TO HOMOGENEOUS POTENTIALS

A. s-wave scattering by repulsive potentials

For a homogeneous repulsive potential,

$$U(r) = U_\alpha^{\mathrm{rep}}(r) = \frac{\hbar^2}{2M}\frac{(\beta_\alpha)^{\alpha-2}}{r^\alpha}, \quad \alpha > 2, \tag{76}$$

the regular zero-energy solution of Eq. (2) (for $m=0$) is essentially a modified Bessel function of the argument

$$z = 2\nu\left(\frac{\beta_\alpha}{r}\right)^{1/(2\nu)}, \quad \nu = \frac{1}{\alpha-2}, \tag{77}$$

namely,

$$u_{\mathrm{reg}}^{(0)}(r) = -2\nu\sqrt{r}K_0(z). \tag{78}$$

For large r (small z), its asymptotic behavior is

$$u_{\mathrm{reg}}^{(0)}(r) \overset{r\to\infty}{\sim} -\sqrt{r}\left[\ln\left(\frac{r}{\beta_\alpha}\right) - 2\nu[\gamma_{\mathrm{E}} + \ln(\nu)]\right]. \tag{79}$$

Comparing with Eq. (11) shows that the scattering length a^{rep} for the repulsive homogeneous potential (76) is

$$a^{\mathrm{rep}} = \nu^{2\nu}\exp(2\nu\gamma_{\mathrm{E}})\beta_\alpha. \tag{80}$$

The leading near-threshold behavior of the s-wave phase shift is given by Eq. (10),

$$\cot\delta \overset{k\to 0}{\sim} \frac{2}{\pi}L(ka^{\mathrm{rep}}), \tag{81}$$

with the logarithmic function L as defined in Eq. (13). According to Eq. (14), the zero of $L(ka^{\mathrm{rep}})$ occurs for

$$ka^{\mathrm{rep}} = x_0 = 2e^{-\gamma_{\mathrm{E}}} \Rightarrow k\beta_\alpha = \frac{2e^{-(1+2\nu)\gamma_{\mathrm{E}}}}{\nu^{2\nu}} \overset{\mathrm{def}}{=} x_\alpha. \tag{82}$$

The effective range is obtained via Eq. (24) from the wave functions $u_{\mathrm{reg}}^{(0)}(r)$ and $v^{(0)}(r) = -\sqrt{r}\ln(r/a^{\mathrm{rep}})$,

$$(r_{\mathrm{eff}}^{\mathrm{rep}})^2 = 2\int_0^\infty [(v^{(0)}(r))^2 - (u_{\mathrm{reg}}^{(0)}(r))^2]dr = \frac{[\nu^\nu\Gamma(1-2\nu)]^4}{2\Gamma(1-4\nu)}\beta_\alpha^2. \tag{83}$$

Numerical values of a^{rep} and $(r_{\mathrm{eff}}^{\mathrm{rep}})^2$ are listed in Table I for integer values of $\alpha > 2$. Note that a finite value of $(r_{\mathrm{eff}}^{\mathrm{rep}})^2$

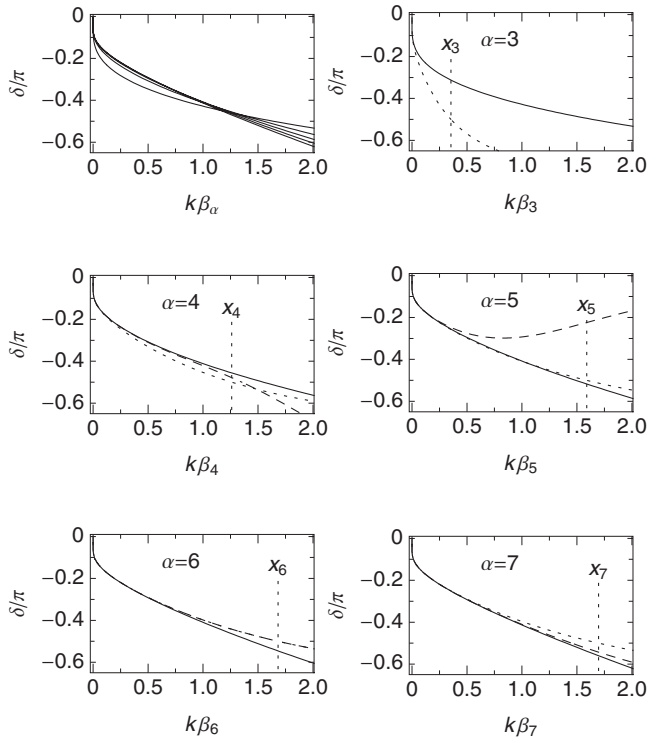

FIG. 1. Phase shifts for s-wave scattering by a homogeneous repulsive potential (76) in two dimensions. Numerically calculated phase shifts for $\alpha=3$ to $\alpha=7$ are shown in the top left panel, from bottom to top (for $k\beta_\alpha \lesssim 1$). In the other panels, each corresponding to a given power α, the numerically calculated phase shifts (solid lines) are compared with the leading behavior (81) (dotted lines), while the dashed lines show the prediction of the effective-range expansion (23) (for $\alpha>4$) or of the modified effective-range expansion (119) (for $\alpha=4$). The vertical dotted lines show the position $k\beta_\alpha=x_\alpha$, where the logarithmic function $L(ka^{\mathrm{rep}})$ is zero according to Eq. (82).

exists only for $\alpha>4$ (see Sec. VII), and that $(r_{\mathrm{eff}}^{\mathrm{rep}})^2$ is negative for $\alpha<6$.

The near-threshold behavior of the phase shifts for scattering by the homogeneous repulsive potentials (76) is illustrated in Fig. 1. The top left panel shows the numerically calculated phase shifts for several powers α; from bottom to top (for $k\beta_\alpha \lesssim 1$) the curves show the results for $\alpha=3$ to $\alpha=7$. The other five panels show, each for a given power α, the numerically calculated phase shifts (solid lines) together with the leading contribution (81) (dotted lines). For $\alpha=5$ to $\alpha=7$ the dashed lines show the results of the effective-range expansion (23), while for $\alpha=4$ the dashed line is the result of the modified effective-range expansion (119), as derived in Sec. VII below. The vertical dotted lines show the position $k\beta_\alpha=x_\alpha$, where the logarithmic function $L(ka^{\mathrm{rep}})$ is zero according to Eq. (82).

The leading contribution (81) clearly reproduces the sudden near-threshold decrease of the phase shifts. Inclusion of the modified effective-range contribution according to Eq. (119) improves the agreement over a larger range of values of $k\beta_\alpha$ for $\alpha=4$, but for $\alpha=5$ the effective range formula (23) leads to much worse agreement for $k\beta_5 \gtrsim 0.4$. Note that $(r_{\mathrm{eff}}^{\mathrm{rep}})^2$ has a large negative value in this case. To verify that

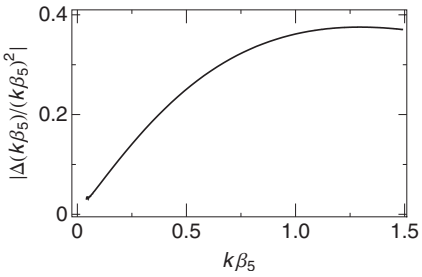

FIG. 2. Difference (84) between the numerically calculated phase shift and the prediction of the effective-range expansion (23) for scattering by the repulsive potential (76) with $\alpha=5$. The curve represents the absolute value of the difference (84) divided by $(k\beta_5)^2$.

the effective-range expansion (23) is nevertheless valid up to and including $O(k^2)$, we plot in Fig. 2 the absolute value of the difference

$$\Delta(k\beta_5) = \delta_{\mathrm{eff.range}}(k\beta_5) - \delta_{\mathrm{num}}(k\beta_5) \tag{84}$$

between the prediction of Eq. (23) and the numerically calculated phase shift, divided by $(k\beta_5)^2$. The curve in Fig. 2 tends smoothly to zero as $k\beta_5 \to 0$, showing that the difference (84) is of higher order than $(k\beta_5)^2$.

For $\alpha=6$ we have $(r_{\mathrm{eff}}^{\mathrm{rep}})^2=0$, so the effective-range expansion up to and including $O(k^2)$ gives the same result as the leading contribution (81). For $\alpha=7$, the leading contribution (81) is still accurate to within 0.016π for $k\beta_7 \approx 1$, and with the effective-range formula (23) the error is smaller still by more than a further factor of 5. Similar or better accuracy is obtained for higher powers α.

B. Quantum reflection by attractive potentials

For an attractive homogeneous potential tail,

$$U_{\mathrm{tail}}(r) = U_\alpha^{\mathrm{att}}(r) = -\frac{\hbar^2}{2M}\frac{(\beta_\alpha)^{\alpha-2}}{r^\alpha}, \quad \alpha>2, \tag{85}$$

the appropriately normalized zero-energy solution of Eq. (2) (with $m=0$) obeying incoming boundary conditions is essentially a Hankel function of the argument z given in Eq. (77), namely,

$$\mathfrak{u}^{(0)}(r) = -i\pi\nu\sqrt{r}H_0^{(1)}(z) \overset{r\to\infty}{\sim} -i\pi\nu\sqrt{r} - \sqrt{r}\left[\ln\left(\frac{r}{\beta_\alpha}\right) - 2\nu[\gamma_{\mathrm{E}} + \ln(\nu)]\right]. \tag{86}$$

Comparing with the asymptotics as expressed in Eq. (27) in terms of the complex scattering length $\mathfrak{a}$ shows that

$$|\mathfrak{a}| = \nu^{2\nu}\exp(2\nu\gamma_{\mathrm{E}})\beta_\alpha, \quad \arg(\mathfrak{a}) = -\pi\nu. \tag{87}$$

The difference between the complex wave function $\mathfrak{u}^{(0)}(r)$, Eq. (86), and the real wave function $u_{\mathrm{reg}}^{(0)}(r)$, Eqs. (78) and (79), is merely that the real parameter β_α in Eqs. (78) and (79) is replaced by $\beta_\alpha e^{-i\pi\nu}$; this is precisely the transformation which transforms the repulsive homogeneous poten-

tial (76) into the attractive potential tail (85), and at the same time transforms the regular behavior of $u_{\mathrm{reg}}^{(0)}(r)$ near the origin into incoming boundary conditions for $\mathfrak{u}^{(0)}(r)$. As already discussed in connection with quantum reflection by homogeneous potential tails for s waves in three dimensions [14], complex lengths characteristic of quantum reflection are obtained from the corresponding real lengths describing conventional scattering by the repulsive homogeneous potential via the transformation

$$\beta_\alpha \to \beta_\alpha e^{-i\pi\nu}, \quad \beta_\alpha^2 \to \beta_\alpha^2 e^{-2i\pi\nu}. \tag{88}$$

Thus

$$\mathfrak{a} = a^{\mathrm{rep}} e^{-i\pi\nu}, \quad |\mathfrak{a}| = a^{\mathrm{rep}}, \tag{89}$$

and for the integral in Eq. (29), which is the square of a length,

$$\mathfrak{r}_{\mathrm{eff}}^2 = 2\int_0^\infty [(\mathfrak{v}^{(0)}(r))^2 - (\mathfrak{u}^{(0)}(r))^2]dr = (r_{\mathrm{eff}}^{\mathrm{rep}})^2 e^{-2i\pi\nu}$$
$$= \frac{[\nu^\nu \Gamma(1-2\nu)]^4}{2\Gamma(1-4\nu)} \beta_\alpha^2 e^{-2i\pi\nu}. \tag{90}$$

Numerical values of the real part $\mathrm{Re}[\mathfrak{r}_{\mathrm{eff}}^2]$ and of the imaginary part $\mathrm{Im}[\mathfrak{r}_{\mathrm{eff}}^2]$ of $\mathfrak{r}_{\mathrm{eff}}^2$ are listed in Table I.

For homogeneous potential tails, we have

$$L(k|\mathfrak{a}|) = \ln\left(\frac{k\beta_\alpha}{2}\right) + \gamma_{\mathrm{E}} + 2\nu[\ln(\nu) + \gamma_{\mathrm{E}}], \tag{91}$$

and the formula (37) becomes

$$R \overset{k\to 0}{\sim} -i\left[1 + \frac{i\pi}{L(k|\mathfrak{a}|) + \frac{1}{2}k^2\,\mathrm{Re}[\mathfrak{r}_{\mathrm{eff}}^2] - i\left(\left[\nu+\frac{1}{2}\right]\pi - \frac{1}{2}k^2\,\mathrm{Im}[\mathfrak{r}_{\mathrm{eff}}^2]\right)}\right]. \tag{92}$$

Including only the leading terms of order k^0 in the expansion (28) for $\cot\mathfrak{d}$, i.e., setting $\mathfrak{r}_{\mathrm{eff}}^2=0$ in Eq. (92), gives the leading behavior of $|R|^2$ as

$$|R|^2 \overset{k\to 0}{\sim} 1 - \frac{2\pi^2\nu}{L(k|\mathfrak{a}|)^2 + \left(\nu+\frac{1}{2}\right)^2\pi^2}, \tag{93}$$

and the leading behavior of the phase of R is

$$\arg(R) \overset{k\to 0}{\sim} -\frac{\pi}{2} + \frac{\pi L(k|\mathfrak{a}|)}{L(k|\mathfrak{a}|)^2 + \arctan\left(\left[\nu^2 - \frac{1}{4}\right]\pi^2\right)}. \tag{94}$$

The probability $|R|^2$ for quantum reflection is shown for various powers α in Fig. 3. In the top left panel, the curves from bottom to top show the numerically calculated values of $|R|^2$ for $\alpha=3$ to $\alpha=7$. In the other panels, each for a given power α, the numerically calculated values of $|R|^2$ (solid lines) are compared with the leading contributions (93) (dotted lines), and the dashed lines show $|R|^2$ as obtained with the effective-range expansion (92) for $\alpha>4$ and with the modified effective-range expansion (115) for $\alpha=4$ (see Sec. VII below).

Figure 3 shows that the probability for quantum reflection tends to unity at threshold, as for s waves in three dimensions, but it drops below unity very rapidly due to the logarithmic denominator in Eq. (93). For a given value of $k\beta_\alpha$, the probability for quantum reflection increases with increasing power α as the potential becomes less smooth.

The argument $\arg(R)$ of the amplitude for quantum reflection by a homogeneous potential tail (85) is shown in Fig. 4. In the top left panel, the curves from bottom to top show the numerically calculated values of $\arg(R)$ for $\alpha=3$ to $\alpha=7$. In the other panels, each for a given power α, the numerically calculated values of $\arg(R)$ (solid lines) are compared with the leading contributions (94) (dotted lines), and the dashed lines show $\arg(R)$ as given by the effective-range expansion (92) for $\alpha>4$ and by the modified effective-range expansion (115) for $\alpha=4$ (see Sec. VII below).

As for the quantum reflection probabilities, the effective-range expansion (92) reproduces the numerically calculated values of $\arg(R)$ quite well, except for $\alpha=5$. For $\alpha=4$, the modified effective-range expansion (115) works well; a spurious drop through π around $k\beta_4 \approx 1.1$ is commented on in Sec. VII below. The derivatives of $\arg(R)$ with respect to energy or wave number can be related to the time shift Δt or the space shift Δr to which an almost monochromatic wave packet is subjected through quantum reflection [31,32]. For example,

$$\Delta r = -\frac{1}{2}\frac{d}{dk}(\arg(R)), \tag{95}$$

meaning that the time evolution of the reflected wave packet corresponds to that of a free wave (free also of the influence of the attractive centrifugal term), which is reflected not at $r=0$ but at $r=\Delta r$. The derivative of $\arg(R)$ with respect to k is negative throughout in Fig. 4, so $\Delta r>0$; the apparent point of reflection lies in front of the origin. This corresponds to a time gain relative to the free particle reflected at $r=0$.

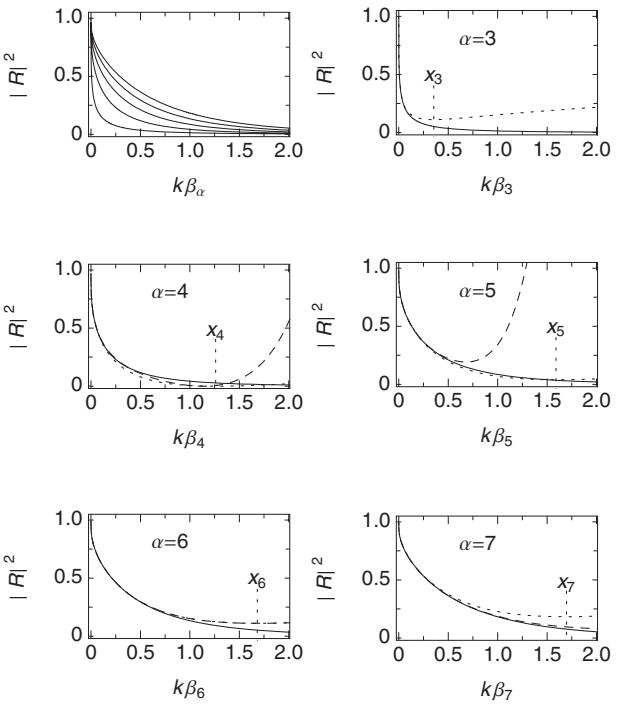

FIG. 3. Probability $|R|^2$ for s-wave quantum reflection by a homogeneous potential (85) in two dimensions. The results for $\alpha=3$ to $\alpha=7$ are shown from bottom to top in the top left panel. In the other panels, each corresponding to a given power α, the solid lines show the numerically calculated quantum reflection probabilities and the dotted lines show the leading contributions (93); the dashed lines show the predictions of the effective-range expansion (92) for $\alpha>4$ and of the modified effective-range expansion (115) for $\alpha=4$. The vertical dotted lines show the position $k\beta_\alpha=x_\alpha$, where the logarithmic function $L(k|\mathfrak{a}|)$ is zero according to Eqs. (82) and (89).

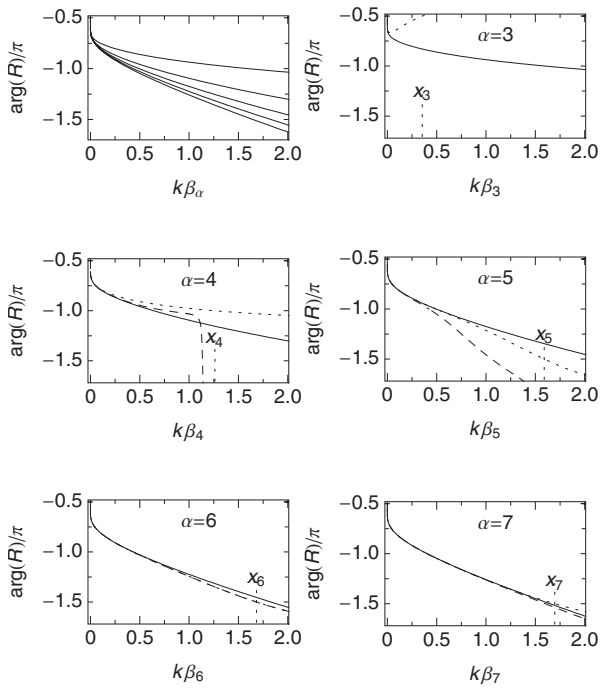

FIG. 4. Argument $\arg(R)$ of the amplitude for s-wave quantum reflection by a homogeneous potential (85) in two dimensions. The results for $\alpha=3$ to $\alpha=7$ are shown from bottom to top in the top left panel. In the other panels, each corresponding to a given power α, the solid lines show the numerically calculated values of $\arg(R)$, the dotted lines show the leading contributions (94), and the dashed lines show the prediction of the effective-range expansion (92) (for $\alpha>4$) or the modified effective-range expansion (115) (for $\alpha=4$). The vertical dotted lines show the position $k\beta_\alpha=x_\alpha$, where the logarithmic function $L(k|\mathfrak{a}|)$ is zero according to Eqs. (82) and (89).

C. Near-threshold quantization

The leading near-threshold behavior of the contribution F_{tail} to the quantization function is determined according to Eqs. (66) and (68), by modulus and argument of the complex scattering length $\mathfrak{a}$, which are given for homogeneous tails in Eq. (87). Equation (68) thus becomes

$$\pi F_{\text{tail}}(E) \overset{\kappa\to 0}{\sim} \arctan\left(-\frac{\pi\nu}{L(\kappa|\mathfrak{a}|)}\right) - \pi\nu\frac{(\kappa\rho_{\text{eff}})^2}{2} + \frac{\pi\nu(\kappa d)^2/2}{\sqrt{(\pi\nu)^2+L(\kappa|\mathfrak{a}|)^2}}, \quad (96)$$

and, in analogy to Eq. (91), the logarithmic function L is

$$L(\kappa|\mathfrak{a}|) = \ln\left(\frac{\kappa\beta_\alpha}{2}\right) + \gamma_{\text{E}} + 2\nu[\ln(\nu)+\gamma_{\text{E}}]. \quad (97)$$

The leading contribution to the right-hand side of Eq. (96), obtained by replacing the arcus tangent by its argument, has already been given in [18]. Remember, however, that all powers of the logarithmic argument of the arcus tangent are essentially of order κ^0.

The subthreshold effective range ρ^2_{eff} is as defined in Eq. (59). The wave function $u^{(0)}$, which tends to $\sqrt{r}$ asymptotically, is

$$u^{(0)}(r) = \sqrt{r}J_0(z), \quad (98)$$

where z is the argument already defined in Eq. (77). According to Eq. (59), ρ^2_{eff} is thus given by

$$\rho^2_{\text{eff}} = 2\int_0^\infty r[1-J_0(z)^2]dr = \frac{(2\nu)^{4\nu}\Gamma(1-2\nu)\Gamma\left(\frac{1}{2}+2\nu\right)}{\sqrt{\pi}\Gamma(1+2\nu)^2}\beta_\alpha^2. \quad (99)$$

Numerical values of ρ^2_{eff} are listed in Table I.

As for s-wave scattering in three dimensions, the scattering length a depends on the absolute positions of near-threshold bound states, and it is not defined for integer values of threshold quantum number n_{th} [see Eq. (74) in Sec. V],

$$a = |\mathfrak{a}|\exp\left(-\frac{\arg(\mathfrak{a})}{\tan(\pi n_{\text{th}})}\right). \quad (100)$$

In contrast to the three-dimensional case, however, a is always positive. As n_{th} increases a little above an integer value, n_0, say, a decreases from $+\infty$, similar to the three-dimensional situation. For $n_{\text{th}}=n_0+\frac{1}{2}$ we have $a=|\mathfrak{a}|$. Beyond $n_0+\frac{1}{2}$ the scattering length a decreases uniformly, almost linearly, over a long stretch and then approaches the next integer value n_0+1 very flatly. This is illustrated in Fig. 5, where

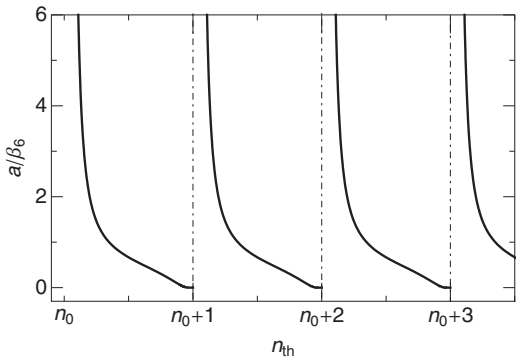

FIG. 5. s-wave scattering length a for a potential well in two dimensions as a function of the threshold quantum number $n_{\rm th}$ according to Eq. (100). For definiteness we have taken parameters corresponding to the homogeneous potential tail (85) with $\alpha=6$ as an example: $|\mathfrak{a}|=0.667\ldots\beta_6$, $\arg(\mathfrak{a})=-\pi/4$.

we have taken parameters corresponding to the homogeneous potential tail (85) with $\alpha=6$ as an example: $|\mathfrak{a}|\approx 0.667\beta_6$, $\arg(\mathfrak{a})=-\frac{\pi}{4}$.

For a bound state very near threshold, the expansion (75) for the scattering length a in terms of the asymptotic inverse penetration depth κ_n is

$$a \overset{\kappa_n\to 0}{\sim} \frac{2e^{-\gamma_{\rm E}}}{\kappa_n} + \kappa_n e^{-\gamma_{\rm E}}\Big(\rho_{\rm eff}^2[(\pi\nu)^2 + L(\kappa|\mathfrak{a}|)^2] - d^2\sqrt{(\pi\nu)^2 + L(\kappa|\mathfrak{a}|)^2}\Big). \tag{101}$$

Among the terms of order κ_n, the leading contribution contains the square $\rho_{\rm eff}^2$ of the subthreshold effective range as given in Table I, and it may be supplemented by a contribution accounting for short-range effects [see the discussion after Eq. (75)]. The second contribution of order κ_n is weaker by $1/\sqrt{L(k|\mathfrak{a}|)^2+(\pi\nu)^2}$, and it contains the coefficient d^2, which is difficult to access in general. In order to verify the structure of Eq. (101), we have solved the Schrödinger equation (2) for Lennard–Jones-type potentials,

$$U_{\rm LJ}(r) = \mathcal{E}\left[\left(\frac{r_{\rm min}}{r}\right)^{2\alpha} - 2\left(\frac{r_{\rm min}}{r}\right)^{\alpha}\right]. \tag{102}$$

The dimensionless strength parameter $B_{\rm LJ}=2M\mathcal{E}(r_{\rm min})^2/\hbar^2$ was varied around 930 for $\alpha=5$, around 1020 for $\alpha=6$, and around 1175 for $\alpha=7$; the highest bound state then has quantum number $n=9$ for $\alpha=5$, $n=7$ for $\alpha=6$, and $n=6$ for $\alpha=7$. A given range of values of $\kappa_n\beta_\alpha$ can be covered by appropriately varying $B_{\rm LJ}$. This allows us to study the behavior of the scattering length as a function of $\kappa_n\beta_\alpha$ in the near-threshold regime. In Fig. 6 we plot the normalized difference,

$$\Delta_\alpha(\kappa_n\beta_\alpha) = -\frac{a - \dfrac{2e^{-\gamma_{\rm E}}}{\kappa_n} - \kappa_n e^{-\gamma_{\rm E}}\{\rho_{\rm eff}^2[(\pi\nu)^2 + L(\kappa|\mathfrak{a}|)^2]\}}{\kappa_n e^{-\gamma_{\rm E}}\sqrt{(\pi\nu)^2 + L(\kappa|\mathfrak{a}|)^2}} \tag{103}$$

of the numerically calculated scattering length a and the known terms on the right-hand side of Eq. (101) as a function of the $\kappa_n\beta_\alpha$. According to Eq. (101), Δ_α should approach d^2 as $\kappa_n\beta_\alpha\to 0$. The numerical results in Fig. 6 are consistent with this expectation and suggest that d^2 is near unity for $\alpha=5$, near -0.2 for $\alpha=7$, and close to zero for $\alpha=6$.

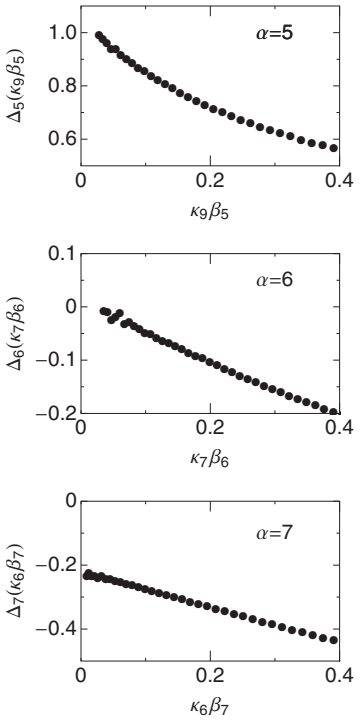

FIG. 6. For the Lennard–Jones-type potential (102), Δ_α represents the normalized difference (103) of the numerically calculated scattering length and the known terms on the right-hand side of Eq. (101). The abscissa is labeled by $\kappa_n\beta_\alpha$, where κ_n is the asymptotic inverse penetration depth of the highest bound state.

Figure 7 shows the scattering length a for the Lennard-Jones potential (102) with $\alpha=6$ as a function of $\kappa_n\beta_6$, $n=7$. The numerically calculated values (dots) are compared with the prediction of the formula (101) with d^2 taken as zero (solid line) and with the leading term alone, $a=2e^{-\gamma_{\rm E}}/\kappa_7$ (dot-dashed line). The divergence for $\kappa_7\beta_6\to 0$ is well described by the leading term, and the improvement due to the term of order κ_7^1 is clearly visible.

VII. POTENTIALS PROPORTIONAL TO $1/r^4$

In this section we describe how the effective-range theory in Secs. II and III can be modified to describe s-wave scattering and quantum reflection by a homogeneous $1/r^4$ potential in two spatial dimensions. The Schrödinger equation (2), with the repulsive potential

$$U^{\rm rep}(r) = \frac{\hbar^2}{2M}\frac{\beta^2}{r^4} \tag{104}$$

and $m=0$ can be transformed via

$$\phi = \frac{u_0}{\sqrt{r}}, \quad y = \ln\left(\frac{r}{\beta}\right), \quad y_0 = \ln\left(\frac{1}{\sqrt{k\beta}}\right),$$

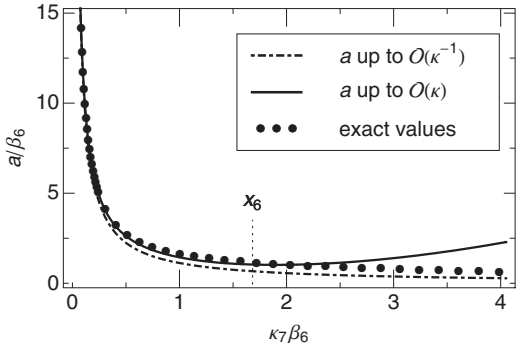

FIG. 7. s-wave scattering length a for the Lennard–Jones-type potential (102) with $\alpha=6$. In the label of the abscissa, κ_7 is the asymptotic inverse penetration depth of the $n=7$ state. The dots are the numerically calculated scattering lengths and the solid line shows the prediction of Eq. (101) when $d^2=0$. The dot-dashed line is the leading term $a=2e^{-\gamma_E}/\kappa_7$.

$$\xi = y - y_0 = \ln\left(\frac{kr}{\sqrt{k\beta}}\right) \tag{105}$$

into

$$\frac{d^2\phi}{d\xi^2} + 2k\beta \sinh(2\xi)\phi(\xi) = 0. \tag{106}$$

In this section, the potentials are always proportional to $1/r^4$, so we drop the subscript "4" on U and on β. For an attractive potential tail

$$U_{\text{tail}}(r) = U^{\text{att}}(r) = -\frac{\hbar^2}{2M}\frac{\beta^2}{r^4}, \tag{107}$$

the same transformations (105) lead to

$$\frac{d^2\phi}{d\xi^2} + 2k\beta \cosh(2\xi)\phi(\xi) = 0. \tag{108}$$

This is essentially Eq. (3.4) in the classic paper by O'Malley, Spruch, and Rosenberg on a modified effective-range theory in three dimensions [33], except that the centrifugal contribution $-(l+\frac{1}{2})^2$ is missing in Eq. (108) above, because s waves in two dimensions ($m=0$) correspond to $l=-\frac{1}{2}$.

Since Eq. (108) has a symmetric potential term, its solutions are easier to handle than those of Eq. (106). One set of solutions consists of the Mathieu functions $M^{(j)}_{\nu_M}(\xi)$ [34], which are labeled by a characteristic parameter ν_M and behave for large positive arguments as

$$M^{(j)}_{\nu_M}(\xi) \overset{\xi\to\infty}{\sim} \mathcal{C}^{(j)}_{\nu_M}(2\sqrt{k\beta}\cosh\xi). \tag{109}$$

Here $\mathcal{C}^{(j)}_{\nu_M}$ stands for a Bessel function, and by convention $j=1,2,3,4$ labels the cases J_{ν_M}, Y_{ν_M}, $H^{(1)}_{\nu_M}$, $H^{(2)}_{\nu_M}$. The characteristic parameter is related to the coefficient $2k\beta$ in front of the cosh term in (108), and for small values,

$$\nu_M \overset{k\beta\to 0}{\sim} \frac{k\beta}{\sqrt{2}} + O([k\beta]^3). \tag{110}$$

From Eq. (105) we see that $\xi\to-\infty$ corresponds to $r\to 0$ and $\xi\to+\infty$ corresponds to $r\to\infty$. The argument of the Bessel functions in Eq. (109) is

$$2\sqrt{k\beta}\cosh\xi = kr + \frac{\beta}{r}. \tag{111}$$

A solution of Eq. (108) obeying incoming boundary conditions for $r\to 0$ is given by

$$\phi(r) = \sqrt{r}M^{(3)}_{\nu_M}(-\xi) \overset{r\to 0}{\sim} \sqrt{r}H^{(1)}_{\nu_M}\left(\frac{\beta}{r}\right). \tag{112}$$

For large r we have $\xi\to\infty$, and the wave function (112) can be matched via

$$M^{(3)}_{\nu_M}(-\xi) \overset{r\to\infty}{\propto} M^{(4)}_{\nu_M}(\xi) + R_{\nu_M}M^{(3)}_{\nu_M}(\xi) \equiv H^{(2)}_{\nu_M}(kr) + R_{\nu_M}H^{(1)}_{\nu_M}(kr) \tag{113}$$

to a superposition of an incoming and a reflected wave at large r. According to [34] we have

$$R_{\nu_M} = -\frac{1}{2}\left[\frac{M^{(4)}_{\nu_M}(0)}{M^{(3)}_{\nu_M}(0)} + \frac{M^{(4)\prime}_{\nu_M}(0)}{M^{(3)\prime}_{\nu_M}(0)}\right]. \tag{114}$$

Due to the additional phase $\pm(\frac{1}{2}\nu_M+\frac{1}{4})\pi$ in the asymptotic (large kr) behavior of the Hankel functions, the quantum reflection amplitude R defined according to Eq. (25) is $R=-iR_{\nu_M}\exp(-i\pi\nu_M)$. From the formulas given in [34] we obtain

$$R \overset{k\to 0}{\sim} -i\frac{L(k|\mathfrak{a}|)}{L(k|\mathfrak{a}|) - i\pi} + \pi(k\beta)^2\frac{3 - 4\zeta(3) - \pi^2L(k|\mathfrak{a}|) - 3i\pi L(k|\mathfrak{a}|)^2 + 2L(k|\mathfrak{a}|)^3}{12[L(k|\mathfrak{a}|) - i\pi]^2}, \tag{115}$$

where ζ stands for the Riemann zeta function and $L(k|\mathfrak{a}|)=2\gamma_E+\ln(k\beta/4)=\ln(k\beta)+2(\gamma_E-\ln 2)$, corresponding to Eq. (91) when $\alpha=4$, $\nu=\frac{1}{2}$. The contribution of the first term on the right-hand side of Eq. (115) (i.e., on the upper line) yields $|R|^2$ and $\arg(R)$ in agreement with Eqs. (93) and (94). The lower line of Eq. (115) modifies the second-order term in the effective-range expansion as necessary for the case $\alpha=4$. As has already been shown in Figs. 3 and 4 in Sec. VI B, Eq. (115) quite accurately reproduces the behavior of the quantum reflection probability and of $\arg(R)$ for an appreciable range of values of $k\beta_4$, and it is definitely an improvement over the predictions of the leading terms (93) and (94) alone. Around $k\beta_4\approx 1.1$, there is a spurious smooth but rather steep drop through π in the prediction of Eq. (115) for $\arg(R)$. For larger values of $k\beta_4$, Eq. (115) predicts a value of $\arg(R)$ very close to zero (modulo 2π), whereas the exact, numerically calculated value is close to $-\pi$.

The results derived above for quantum reflection by the attractive potential are readily transferred to the case of scat-

TABLE II. Power τ representing the order of the first term not included in Eq. (130) describing the leading near-threshold behavior of tan $\delta_{m>0}$ in the noncritical cases.

$\alpha<2m$	$\alpha=5$	$3\leqslant m$	$\tau=5$
		$m<3$	$\tau=7$
	$\alpha\geqslant 6$		$\tau=\alpha+2$
$\alpha=2m$			$\tau=2m+2$
$2m<\alpha<2m+2$	$\alpha=5$	$m\leqslant 2$	$\tau=5$
		$2<m$	$\tau=7$
	$\alpha\geqslant 6$		$\tau=\alpha+2$
$2m+2<\alpha<2m+4$	$\alpha=5$		$\tau=2m+3$
	$\alpha\geqslant 6$		$\tau=2m+4$
$2m+4<\alpha$		$m<1$	$\tau=2m+2$
		$m>1$	$\tau=\min\{\alpha+2,4m,2m+4\}$

tering by the repulsive potential. The transformation which changes the attractive potential (107) into the repulsive potential (104) and incoming boundary conditions for the wave function into regularity near the origin is

$$\beta \to \beta e^{+i\pi\nu} = i\beta \tag{116}$$

[cf. Eq. (88)]. The logarithmic function $L(k|\mathfrak{a}|)=L(ka^{\rm rep})=\ln(\frac{1}{2}ka^{\rm rep})+\gamma_{\rm E}$ occurring in formulas for scattering by the repulsive potential (104) is replaced by $\ln(\frac{1}{2}ka^{\rm rep})-i\frac{\pi}{2}+\gamma_{\rm E}$ for the corresponding formulas for quantum reflection by the attractive potential tail (107). The reverse transformation is achieved by replacing $\ln(\frac{1}{2}ka^{\rm rep})+\gamma_{\rm E}$ with $\ln(\frac{1}{2}ka^{\rm rep})+i\frac{\pi}{2}+\gamma_{\rm E}$. In order to transform the expression (115) for the quantum reflection amplitude by the attractive potential tail (107) to the reflection amplitude for scattering by the repulsive potential (104), we have to apply, in addition to Eq. (116), the transformation

$$L(k|\mathfrak{a}|) \to L(k|\mathfrak{a}|) + i\frac{\pi}{2}. \tag{117}$$

Applying Eqs. (116) and (117) to Eq. (115) gives the following expression for the S matrix, $S_{m=0}=iR$ [compare Eqs. (25) and (26)] for scattering by the repulsive potential (104):

$$S_{m=0} \overset{k\to 0}{\sim} \frac{L(k|\mathfrak{a}|)+i\frac{\pi}{2}}{L(k|\mathfrak{a}|)-i\frac{\pi}{2}} - i\pi(k\beta)^2 \frac{3-4\zeta(3)+\frac{\pi^2}{2}L(k|\mathfrak{a}|)+2L(k|\mathfrak{a}|)^3}{12\left[L(k|\mathfrak{a}|)-i\frac{\pi}{2}\right]^2}. \tag{118}$$

It is easy to verify that the modulus of $S_{m=0}=e^{2i\delta}$ is unity to order below $(k\beta)^4$, and the cotangent of the real phase shift δ can be obtained via $\cot\delta=-i(1+S_{m=0})/(1-S_{m=0})$ as

$$\cot\delta \overset{k\to 0}{\sim} \frac{2}{\pi}\left[L(k|\mathfrak{a}|)+\frac{(k\beta)^2}{2}\left(\frac{1}{2}-\frac{2}{3}\zeta(3)+\frac{\pi^2}{12}L(k|\mathfrak{a}|)+\frac{1}{3}L(k|\mathfrak{a}|)^3\right)\right]. \tag{119}$$

In order to verify that Eq. (119) is the correct expansion up to the order $O(k^2)$, we plot in Fig. 8 the absolute value of the difference

$$\Delta(k\beta_4) = \delta_{\rm eff.range}(k\beta_4) - \delta_{\rm num}(k\beta_4) \tag{120}$$

between the prediction of Eq. (119) and the numerically calculated phase shift, divided by $(k\beta_4)^2$. The curve in Fig. 8 tends smoothly to zero as $k\beta_4\to 0$, showing that the difference (120) is of higher order than $(k\beta_4)^2$. As has already been shown in Fig. 1 in Sec. VI A, Eq. (119) quite accurately reproduces the behavior of the s-wave phase shift for an appreciable range of values of $k\beta_4$, and it is definitely an improvement over the predictions of the leading term (81) alone.

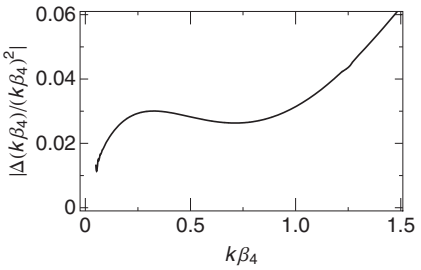

FIG. 8. Difference (120) between the numerically calculated phase shift and the prediction of the effective-range expansion (119) for scattering by the repulsive potential (104). The curve represents the absolute value of the difference (120) divided by $(k\beta_4)^2$.

VIII. NONVANISHING ANGULAR MOMENTUM

For $m\neq 0$, the two threshold solutions of the free radial Schrödinger equation (2), proportional to $r^{(1/2)\pm|m|}$, are linearly independent, and many results from the three-dimensional case can be transferred to the two-dimensional case by writing $|m|-\frac{1}{2}$ for l. Del Giudice and Galzenati [35,36] determined the leading and next-to-leading terms in the near-threshold behavior of the phase shifts δ_l for the three-dimensional radial Schrödinger equation with a homogeneous repulsive potential (76) using the theory of Jost functions and a matching method [37] to fit the Jost solutions to the regular solution at small distances. In a recent paper [38] we have shown that this theory can be extended to the case of attractive singular potentials (85) and incoming boundary conditions via the transformation (88). The work in [35,36] and in [38] was restricted to integer l, but this restriction is not essential. Noninteger "angular momentum" quantum numbers play a role whenever the potential energy term contains an inverse-square contribution, whose origin is *not* related to angular momentum. An example is the interaction

of a point charge with a dipole. In this section we present results for the Schrödinger equation (2) with arbitrary not (necessarily) integer $m \neq 0$, i.e., the "centrifugal" potential may be attractive, but it is less attractive than the centrifugal potential for s waves in two dimensions. Since the radial Schrödinger equation (2) does not depend on the sign of m, we assume $m > 0$, i.e., $l = m - \frac{1}{2} > -\frac{1}{2}$.

In order to calculate the phase shifts δ_m for $m > 0$ for the repulsive potential (76), we follow the steps in [35] and express the solutions $u_m(r)$ of Eq. (2) in terms of the S matrix $S_m = e^{2i\delta_m}$ [see Eq. (15)] and the Jost solutions [39] $f_\pm(k,r)$, which are irregular solutions defined via the boundary conditions $e^{\mp ikr} f_\pm(k,r) \overset{r\to\infty}{\to} 1$,

$$u_m(r) = A[f_-(k,r) - ie^{-i\pi m} S_m(k) f_+(k,r)], \tag{121}$$

[cf. Eq. (6) in Sec. II]. If the exact regular solution $u_{\mathrm{reg},m}(k,r)$ of Eq. (2) is known for $r \leqslant r_0$ (with an arbitrary finite r_0), then the Jost solution can be matched to the regular solution at $r = r_0$ via the logarithmic derivatives,

$$\left.\frac{u'_{\mathrm{reg},m}}{u_{\mathrm{reg},m}}\right|_{r=r_0} = \left.\frac{f'_-(k,r) - ie^{-i\pi m} S_m(k) f'_+(k,r)}{f_-(k,r) - ie^{-i\pi m} S_m(k) f_+(k,r)}\right|_{r=r_0}, \tag{122}$$

and the Jost functions $\mathcal{F}_\pm(k)$ can be defined as the Wronskian determinants of the respective Jost solution $f_\pm$ and the exact solution $u_{\mathrm{reg},m}$,

$$\mathcal{F}_\pm(k) = W[f_\pm(k,r), u_{\mathrm{reg},m}(k,r)]|_{r=r_0}. \tag{123}$$

The S matrix is related to the Jost functions via

$$S_m(k) = e^{2i\delta_m} = ie^{-i\pi m} \frac{\mathcal{F}_-(k)}{\mathcal{F}_+(k)}, \tag{124}$$

so the phase shifts are given by

$$\tan\delta_m = \frac{\mathrm{Im}\left\{\mathcal{F}_-(k)\exp\left[i\pi\left(\frac{m}{2} - \frac{1}{4}\right)\right]\right\}}{\mathrm{Re}\left\{\mathcal{F}_-(k)\exp\left[i\pi\left(\frac{m}{2} - \frac{1}{4}\right)\right]\right\}}. \tag{125}$$

Many different approaches can be found to calculate the Jost solutions, e.g., [40]. For the special case of homogeneous potentials, $f_-(k,r)$ can be found by transforming the radial Schrödinger equation into a corresponding integral equation [see Eq. (32) in [38]], which can be solved iteratively and provides a power expansion of $f_-(k,r)$. With the substitutions

$$z = k^{2/\alpha}\beta_\alpha^{-(\alpha-2)/\alpha} r, \quad q = (k\beta_\alpha)^{(\alpha-2)/\alpha} \quad \text{and} \quad \eta = 2\nu, \tag{126}$$

we get the following expression for $f_-(q,z)$:

$$\begin{aligned} f_-(q,z) = &-\frac{1}{\sqrt{2\pi}} \exp\left(-\frac{3}{4}\pi i\right) q^{1/2} \left\{ \exp\left(-\frac{1}{2} m\pi i\right) \Gamma(m) 2^m z^{-m+1/2} \right. \\ &\times \left[q^{-m} + \frac{1}{4}\left(\frac{\eta^2}{1+\eta m} z^{-2/\eta} - \frac{1}{1-m} z^2\right) q^{-m+2} + \frac{1}{4\sqrt{\pi}} \frac{\Gamma(-1/\eta)\Gamma(m-1/\eta)\Gamma(1/\eta+1/2)}{\Gamma(1/\eta+m+1)} \exp\left(i\frac{\pi}{\eta}\right) q^{-m+2/\eta+2} + \cdots \right] \\ &+ \exp\left(\frac{1}{2} m\pi i\right) \Gamma(-m) 2^{-m} z^{m+1/2} \\ &\times \left[q^m + \frac{1}{4}\left(\frac{\eta^2}{1-\eta m} z^{-2/\eta} - \frac{1}{1+m} z^2\right) q^{m+2} \right. \\ &\left. \left. + \frac{1}{4\sqrt{\pi}} \frac{\Gamma(-1/\eta)\Gamma(-m-1/\eta)\Gamma(1/\eta+1/2)}{\Gamma(1/\eta-m+1)} \exp\left(i\frac{\pi}{\eta}\right) q^{m+2/\eta+2} + \cdots \right] \right\}. \end{aligned} \tag{127}$$

Near the origin, the regular solution decays exponentially and can be written, with the substitutions given above, as

$$u_m^{\mathrm{reg}}(q,z) \overset{qz\to 0}{\sim} z^{1/2} z^{1/(2\eta)} \exp(-\eta q z^{-1/\eta}). \tag{128}$$

Using a simple transformation [see Eq. (39) in [38]], the series expansion of $u_m^{\mathrm{reg}}(q,z)$ can be found from the corresponding expression of $f_-(q,z)$,

$$\begin{aligned} u_m^{\mathrm{reg}}(q,z) = &\frac{1}{\sqrt{2\pi}} (\eta q)^{1/2} \left\{ \Gamma(\eta m) 2^{\eta m} z^{m+1/2} \left[(\eta q)^{-\eta m} - \frac{1}{4}\left(\frac{1}{\eta^2(m+1)} z^2 - \frac{1}{1-\eta m} z^{-2/\eta}\right)(\eta q)^{-\eta m+2} \right.\right. \\ &\left. - \frac{1}{4\sqrt{\pi}} \frac{\Gamma(-\eta)\Gamma(\eta m-\eta)\Gamma(\eta+1/2)}{\Gamma(\eta+\eta m+1)} (\eta q)^{-\eta m+2\eta+2} + \cdots \right] \\ &+ \Gamma(-\eta m) 2^{-\eta m} z^{-m+1/2} \left[(\eta q)^{\eta m} - \frac{1}{4}\left(\frac{1}{\eta^2(1-m)} z^2 - \frac{1}{\eta m+1} z^{-2/\eta}\right)(\eta q)^{\eta m+2} \right. \end{aligned}$$

$$-\frac{1}{4\sqrt{\pi}}\frac{\Gamma(-\eta)\Gamma(-\eta m-\eta)\Gamma(\eta+1/2)}{\Gamma(\eta-\eta m+1)}(\eta q)^{\eta m+2+2\eta}+\cdots\Bigg]\Bigg\}. \tag{129}$$

With Eq. (125) the tangents $\tan\delta_m$ of the (real) phase shifts can be calculated, remembering that in Eqs. (127) and (129) only terms proportional to $z^{m-1/2}$ and $z^{-m-1/2}$ contribute (see [36] and the discussion within). As in the case of integer l, we have to distinguish between noncritical and critical powers α. For the noncritical cases we get

$$\begin{aligned}\tan\delta_m(k) \overset{k\to 0}{\sim}& \frac{\sqrt{\pi}\Gamma(m-1/(2\nu))\Gamma(1/2+1/(2\nu))}{4\Gamma(1+m+1/(2\nu))\Gamma(1+1/(2\nu))}(k\beta_\alpha)^{\alpha-2}+\frac{2^{-2m}\pi\nu^{4m\nu}\Gamma(-2m\nu)}{\Gamma(m)\Gamma(1+m)\Gamma(2m\nu)}(k\beta_\alpha)^{2m}\\ &-\frac{2^{-4m}\pi\nu^{8m\nu}\cos(m\pi)\Gamma(1-m)\Gamma^2(-2m\nu)}{\Gamma(m)\Gamma^2(1+m)\Gamma^2(2m\nu)}(k\beta_\alpha)^{4m}\\ &+\frac{2^{-2m+4\nu}\pi^{3/2}\nu^{2+4(1+m)\nu}\Gamma(-2\nu)\Gamma(-2m\nu)\Gamma(1/2+2\nu)}{\Gamma(m)\Gamma(1+m)\Gamma(2m\nu)\Gamma(1-2(m-1)\nu)\Gamma(1+2(1+m)\nu)}\\ &\times\{\csc[2(m-1)\pi\nu]+\csc[2(m+1)\pi\nu]\}(k\beta_\alpha)^{2m+2}+O((k\beta_\alpha)^\tau).\end{aligned} \tag{130}$$

Terms in Eq. (130) are to be ignored, if they are of order τ or higher, where τ depends on the power α and on the (not necessarily integer) value $m>0$ as listed in Table II.

The critical cases are easily identified as those cases where the arguments of some of the gamma functions in Eq. (130) are zero or a negative integer. Well-defined results can be obtained for these cases by taking limits as m approaches the critical value. For the critical case $m=1$, which corresponds to the p wave in two dimensions, we get

$$\tan\delta_1(k) \overset{k\to 0}{\sim} -\frac{2}{3}k\beta_3+O((k\beta_3)^2) \quad \text{for } \alpha=3, \tag{131}$$

$$\tan\delta_1(k) \overset{k\to 0}{\sim} \frac{\pi}{8}(k\beta_4)^2\ln(k\beta_4)-\frac{\pi}{32}(1-8\gamma_E+8\ln 2)(k\beta_4)^2+O((k\beta_4)^3) \quad \text{for } \alpha=4, \tag{132}$$

$$\tan\delta_1(k) \overset{k\to 0}{\sim} \frac{3^{5/3}\pi\Gamma(-2/3)}{108\Gamma(2/3)}(k\beta_5)^2+\frac{16}{45}(k\beta_5)^3+O((k\beta_5)^4) \quad \text{for } \alpha=5, \tag{133}$$

$$\tan\delta_1(k) \overset{k\to 0}{\sim} -\frac{\pi}{8}(k\beta_6)^2-\frac{\pi}{16}(k\beta_6)^4\ln((k\beta_6))-\frac{\pi}{384}(-19+36\gamma_E-24\ln 2)(k\beta_6)^4+O((k\beta_6)^6) \quad \text{for } \alpha=6, \tag{134}$$

$$\begin{aligned}\tan\delta_1(k) \overset{k\to 0}{\sim}& \frac{\pi\nu^{4\nu}\Gamma(-2\nu)}{4\Gamma(2\nu)}(k\beta_\alpha)^2-\frac{\pi\nu^{8\nu}\Gamma^2(-2\nu)}{8\Gamma^2(2\nu)}(k\beta_\alpha)^4\ln(k\beta_\alpha)\\ &+\frac{\pi\nu^{8\nu}\Gamma^2(-2\nu)}{8\Gamma^2(2\nu)}\{1-\gamma_E+\ln 2+\pi\nu[\cot(2\pi\nu)+\csc(4\pi\nu)]-\nu[H_{4\nu}+2\ln\nu-2\Psi(2\nu)]\}(k\beta_\alpha)^4\\ &+O((k\beta_\alpha)^5) \quad \text{for } \alpha>6,\end{aligned} \tag{135}$$

with the harmonic number H_n, which is defined via the integral

$$H_n=\int_0^1\frac{1-x^n}{1-x}dx. \tag{136}$$

For the critical case $\alpha_{\text{crit}}=2m+2$,

$$\begin{aligned}\tan\delta_m(k) \overset{k\to 0}{\sim}& \frac{2^{-1-2m}\pi}{\Gamma^2(1+m)}\ln(k\beta_{2m+2})(k\beta_{2m+2})^{2m}-\frac{2^{-1-2m}\pi}{m\Gamma^2(1+m)}\{(1+m)[\ln(2)-\gamma_E]+m(H_m-1/2H_{2m})+\ln m\}(k\beta_{2m+2})^{2m}\\ &-\frac{2^{-3-2m}m^{-6-2/m}\pi^{3/2}\Gamma^2(-1/m)\Gamma(-(1+m)/m)}{\Gamma(1/2-1/m)\Gamma^2(m)}(k\beta_{2m+2})^{2m+2}+O((k\beta_{2m+2})^\tau),\end{aligned} \tag{137}$$

with $\tau=6$ for $\alpha=5$ and $\tau=2m+4$ for $\alpha\geqslant 6$.

For the critical case $\alpha_{\text{crit}}=2m+4$,

$$\tan\delta_m(k) \overset{k\to 0}{\sim} \frac{2^{-2m(2+m)/(1+m)}(1+m)^{-2m/(1+m)}\pi\Gamma(-1+1/(1+m))}{\Gamma(m)\Gamma(m/(1+m))\Gamma(1+m)}(k\beta_{2m+4})^{2m} - \frac{2^{-2-2m}\pi}{\Gamma(1+m)\Gamma(2+m)}(k\beta_{2m+4})^{2m+2}\ln(k\beta_{2m+4})$$
$$+ \frac{2^{-3-2m}\pi}{\Gamma^2(2+m)}\left[3+\frac{m^2+1}{m}-(2+m)\gamma_E+(2m+4)\ln 2+2\ln(1+m)+\pi\csc\left(\frac{(m-1)\pi}{m+1}\right)+2(1+m)\Psi(m)\right.$$
$$\left.-\Psi\left(\frac{2}{1+m}\right)+\Psi\left(\frac{m}{1+m}\right)+\Psi\left(-1+\frac{1}{1+m}\right)-(1+m)\Psi(2+2m)\right](k\beta_{2m+4})^{2+2m}$$
$$+ O((k\beta_{2m+4})^{2m+4}). \tag{138}$$

For $\alpha_{\text{crit}}=3$ and $m>0$, Eq. (125) reduces to

$$\tan\delta_m(k) \overset{k\to 0}{\sim} \frac{2^{-2m}\pi\Gamma(-2m)}{\Gamma(m)\Gamma(2m)\Gamma(1+m)}(k\beta_3)^{2m} - \frac{2}{4m^2-1}k\beta_3$$
$$+ \frac{2^{-2m}\sqrt{\pi}\cos(m\pi)\Gamma(-1-2m)\Gamma(1-m)\Gamma(-2m)\Gamma(3/2+m)}{\Gamma^3(2m)\Gamma^2(1+m)}(k\beta_3)^{4m} + O((k\beta_3)^{\tau}), \tag{139}$$

with a remainder of order $\tau=1$ for $0<m<\frac{1}{4}$, $\tau=\frac{3}{2}$ for $m=\frac{1}{4}$, $\tau=4m$ for $\frac{1}{4}<m<\frac{1}{2}$, and $\tau=2$, if $m>\frac{1}{2}$. For $m=\frac{1}{2}$, which corresponds to the s-wave contribution in three dimensions we get [see Eq. (12′) in [35]]

$$\tan\delta_{1/2}(k) \overset{k\to 0}{\sim} (k\beta_3)\ln(k\beta_3) + \left(\ln 2+3\gamma-\frac{3}{2}\right)(k\beta_3)$$
$$+ O((k\beta_3)^2).$$

And finally, for $\alpha_{\text{crit}}=4$,

$$\tan\delta_m(k) \overset{k\to 0}{\sim} \frac{2^{-4m}\pi\Gamma(-m)}{\Gamma^2(m)\Gamma(1+m)}(k\beta_4)^{2m} - \frac{\pi}{8m(m^2-1)}(k\beta_4)^2$$
$$+ \frac{2^{-8m}\pi^2\cot(m\pi)\Gamma(1-m)\Gamma(-m)}{\Gamma^3(m)\Gamma^3(1+m)}(k\beta_4)^{4m}$$
$$+ O((k\beta_4)^{\tau}), \tag{140}$$

with a remainder of order $\tau=1$ for $0<m<\frac{1}{4}$, $\tau=\frac{3}{2}$ for $m=\frac{1}{4}$, $\tau=2$ for $\frac{1}{4}<m<\frac{1}{2}$, $\tau=4m+2$ for $\frac{1}{2}<m<1$, $\tau=4$ for $1<m\leqslant\frac{3}{2}$, $\tau=3$ for $\frac{3}{2}<m<2$, and $\tau=4$ for $m\geqslant 2$.

For the special case $m=\frac{1}{2}$, which corresponds to the s-wave contribution in three dimensions, we get [see Eq. (12′) in [35]]

$$\tan\delta_{1/2}(k) \overset{k\to 0}{\sim} -(k\beta_4)+\frac{\pi}{3}(k\beta_4)^2+\frac{4}{3}(k\beta_4)^3\ln(k\beta_4)$$
$$+\left(\frac{8}{3}(\gamma_E+\ln 2)-\frac{28}{9}\right)(k\beta_4)^3+O((k\beta_4)^4). \tag{141}$$

For attractive singular potentials the Schrödinger equation (2) can be solved with incoming boundary conditions for $r\to 0$, where the WKB approximation becomes increasingly accurate. When $m>\frac{1}{2}$, the centrifugal potential is repulsive and contributes to a genuine potential barrier. In this case, reflection at near-threshold energies is not "quantum reflection," but classically allowed reflection, and any deviation of the reflection probability from unity at sub-barrier energies is due to (quantum) tunneling through the potential barrier. The formalism described in Sec. III is essentially independent of whether the "centrifugal term" is attractive or repulsive. The incoming boundary conditions describe total absorption at small distances [14]. The S matrix $S_m=\exp(2i\mathfrak{d}_m)$ is no longer necessarily unitary and the reflection amplitude $R_m=-(-1)^m iS_m$ [cf. Eqs. (6) and (25) in Secs. II and III] is given by the complex phase shift in analogy to Eq. (26),

$$R_m=-(-1)^m i\frac{\cot\mathfrak{d}_m+i}{\cot\mathfrak{d}_m-i}. \tag{142}$$

For homogeneous attractive potentials (85), the near-threshold behavior of the complex phase shifts $\mathfrak{d}_m$ can be derived from the analytical expressions for the real phase shifts for scattering by the repulsive homogeneous potential (76) by simply applying the transformation (88). For example, for the critical case $\alpha_{\text{crit}}=4$ we get

$$\tan\mathfrak{d}_m(k) \overset{k\to 0}{\sim} \frac{2^{-4m}\pi\Gamma(-m)}{\Gamma^2(m)\Gamma(1+m)}(k\beta_4)^{2m}e^{-im\pi}$$
$$-\frac{\pi}{8m(m^2-1)}(k\beta_4)^2e^{-i\pi}$$
$$+\frac{2^{-8m}\pi^2\cot(m\pi)\Gamma(1-m)\Gamma(-m)}{\Gamma^3(m)\Gamma^3(1+m)}(k\beta_4)^{4m}e^{-2im\pi}$$
$$+O((k\beta_4)^{\tau}), \tag{143}$$

where τ is defined as above.

As a last point we wish to comment on the effective-range expansion we formulated for nonvanishing angular momentum in [38] [see Eqs. (53) and (54) in that paper]. In terms of $m\equiv l+\frac{1}{2}$, Eq. (53) of [38] becomes

$$k^{2m}\cot(\delta_m(k)) = -\frac{1}{a_l^{2m}} + \frac{1}{2}r_{\mathrm{eff},m}^{2-2m}k^2. \tag{144}$$

From Eq. (130) above, we see that this form is only valid for $m>1$. For $m<1$ there is an additional term of order k^{2m}, which vanishes for $m=\frac{1}{2}$.

IX. SUMMARY AND DISCUSSION

We have presented a detailed and comprehensive description of scattering, quantum reflection and near-threshold quantization for circularly symmetric potentials in two spatial dimensions. In contrast to the one- and three-dimensional cases, the radial Schrödinger equation (2) contains a centrifugal term $\hbar^2(m^2-\frac{1}{4})/(2Mr^2)$, which is nonzero for all integer m, even for s waves, $m=0$. The near-threshold behavior of scattering phase shifts, quantum reflection amplitudes, and quantization functions is dominated by a logarithmic dependence on the wave number k (above threshold) or the asymptotic inverse penetration depth κ (below threshold). The effective-range theory known from three-dimensional systems can be adapted to scattering in two dimensions by an appropriate definition of the scattering length a and a quantity r_{eff}^2, which has the dimensions of a length squared and can be called an effective range squared. The appropriate effective range expansion for the cotangent of the s-wave phase shift is given quite generally by Eq. (23), as already formulated by Verhaar *et al.* [11]. In contrast to the situation in three dimensions, the scattering length a is always positive when defined, i.e., when there is not a bound state exactly at threshold, and r_{eff}^2 can be negative.

The results for elastic scattering can be adapted to the case of (quantum) reflection by a singular attractive potential tail by imposing incoming boundary conditions at small distances, where the WKB approximation becomes increasingly accurate. This is an unambiguous description of total absorption at small distances. The S matrix is now no longer necessarily unitary, and the s-wave phase shift $\mathfrak{d}$ is complex. The effective-range expansion of ordinary scattering theory is adapted to describe the near-threshold behavior of the complex phase shift and the amplitude for quantum reflection in terms of a complex scattering length $\mathfrak{a}$ and a complex effective range squared $\mathfrak{r}_{\mathrm{eff}}^2$ [see Eqs. (28), (36), and (37)].

Below threshold, the leading and next-to-leading behavior of the quantization function $F(E)$, which defines the position of near-threshold bound states according to the quantization rule (38), $n_{\mathrm{th}}-n=F(E_n)$, are derived with a subthreshold effective-range theory, as done recently for the three-dimensional case in [15,16]. The near-threshold behavior of $F(E)$ is dominated up to $O(E)$ by the contribution F_{tail} of the potential tail as described in Eq. (68). From the leading logarithmic term [see also Eq. (66)],

$$F(E) \overset{\kappa\to 0}{\sim} F_{\mathrm{tail}}(E) \overset{\kappa\to 0}{\sim} \frac{1}{\pi}\arctan\left(\frac{\arg(\mathfrak{a})}{L(\kappa|\mathfrak{a}|)}\right), \tag{145}$$

we can derive a relation directly connecting the energy $E=-\hbar^2\kappa_n^2/(2M)$ of a bound state very near threshold to the scattering length a,

$$a = \frac{x_0}{\kappa_n} + O(\kappa_n), \quad x_0 = 2e^{-\gamma_{\mathrm{E}}}. \tag{146}$$

In contrast to s waves in three dimensions, the expansion (146) contains no contribution of order κ_n^0. The term of order κ_n^1 is given in Eq. (75). It contains a large contribution from the subthreshold effective range, which may be slightly modified due to short-range properties of the potential. It also contains a probably smaller contribution, which is more difficult to access and due to the term of order E in the WKB representation of the threshold wave function (71).

The applicability of the effective-range formulas derived for scattering, quantum reflection, and near-threshold quantization for s waves in two dimensions is demonstrated for repulsive homogeneous potentials and for attractive homogeneous potential tails in Sec. VI. Analytical expressions are given for the scattering length (80) and the effective range squared (83) of the repulsive potentials, as well as for the modulus and argument (89) of the complex scattering length and the effective range squared (90) for attractive potential tails. The analytical expression for the subthreshold effective range for attractive homogeneous potential tails is Eq. (99). The modified effective-range theory required for potentials proportional to $1/r^4$ is presented in Sec. VII, and analytical expressions are given for the expansion of the real phase shift (119) in the repulsive case as well as for the quantum reflection amplitude (115) in the attractive case. Numerical values of the parameters determining the near-threshold behavior of phase shifts, etc. are given in Table I.

To complement the extensive treatment of s waves, $m=0$, in Secs. II–VII, Sec. VIII presents various formulas for the leading contributions to the near-threshold behavior of real and complex phase shifts for nonvanishing angular momentum quantum number m. The results of the present paper should be useful for the study of planar scattering problems and of three-dimensional problems with translational invariance in one degree of freedom, such as the scattering of cold atoms or molecules by a conducting or dielectric nanotube. Since the results of Sec. VIII are not restricted to integer or half-integer values of m, they are also applicable to a wide range of other physical situations involving inverse-square potentials, such as monopole-dipole scattering.

ACKNOWLEDGMENTS

We thank Johannes Eiglsperger, Javier Madroñero, and Andrés Naranjo for helpful discussions and carefully reading the manuscript. This work was supported by the Deutsche Forschungsgemeinschaft, AZ: Grant No. Fr-591/13-2.

[1] Yu. Kagan, G. V. Shlyapnikov, I. A. Vartan'yants, and N. A. Glukhov, JETP Lett. **35**, 477 (1982).
[2] M. Papoular, J. Phys. B **18**, L821 (1983).
[3] J. Denschlag, G. Umshaus, and J. Schmiedmayer, Phys. Rev. Lett. **81**, 737 (1998).
[4] M. Bawin and S. A. Coon, Phys. Rev. A **63**, 034701 (2001).
[5] M. A. Cirone, K. Rzazewski, W. P. Schleich, F. Straub, and J. A. Wheeler, Phys. Rev. A **65**, 022101 (2001).
[6] K. Kowalski, K. Podlaski, and J. Rembielinski, Phys. Rev. A **66**, 032118 (2002).
[7] H. Friedrich, *Theoretical Atomic Physics* (Springer-Verlag, Berlin, 2006).
[8] I. R. Lapidus, Am. J. Phys. **50**, 45 (1982).
[9] A. K. Adhikari, Am. J. Phys. **54**, 362 (1986).
[10] Z.-Y. Gu and S. W. Quian, Phys. Lett. A **136**, 6 (1989).
[11] B. J. Verhaar, J. P. H. W. van den Eijnde, M. A. Voermans, and M. M. J. Schaffrath, J. Phys. A **17**, 595 (1984).
[12] R. Côté, H. Friedrich, and J. Trost, Phys. Rev. A **56**, 1781 (1997).
[13] H. Friedrich, G. Jacoby, and C. G. Meister, Phys. Rev. A **65**, 032902 (2002).
[14] F. Arnecke, H. Friedrich, and J. Madroñero, Phys. Rev. A **74**, 062702 (2006).
[15] H. Friedrich and P. Raab, Phys. Rev. A **77**, 012703 (2008).
[16] P. Raab and H. Friedrich, Phys. Rev. A **78**, 022707 (2008).
[17] *Handbook of Mathematical Functions*, edited by M. Abramowitz and I. A. Stegun (Dover Publications, New York, 1972).
[18] M. J. Moritz, C. Eltschka, and H. Friedrich, Phys. Rev. A **63**, 042102 (2001); **64**, 022101 (2001).
[19] J. R. Taylor, *Scattering Theory: The Quantum Theory of Nonrelativistic Collisions* (John Wiley & Sons, New York, 1972).
[20] P. G. Burke, *Potential Scattering in Atomic Physics* (Plenum Press, New York, 1977).
[21] R. G. Newton, *Scattering Theory of Waves and Particles* (Springer-Verlag, Berlin, 1982).
[22] S. K. Adhikari and W. G. Gibson, Phys. Rev. A **46**, 3967 (1992).
[23] H. Friedrich and J. Trost, Phys. Rep. **397**, 359 (2004).
[24] J. Böheim, W. Brenig, and J. Stutzki, Z. Phys. B: Condens. Matter **48**, 43 (1982).
[25] D. P. Clougherty and W. Kohn, Phys. Rev. B **46**, 4921 (1992).
[26] F. Shimizu, Phys. Rev. Lett. **86**, 987 (2001).
[27] A. Mody, M. Haggerty, J. M. Doyle, and E. J. Heller, Phys. Rev. B **64**, 085418 (2001).
[28] T. A. Pasquini, Y. Shin, C. Sanner, M. Saba, A. Schirotzek, D. E. Pritchard, and W. Ketterle, Phys. Rev. Lett. **93**, 223201 (2004).
[29] T. A. Pasquini, M. Saba, G. Jo, Y. Shin, W. Ketterle, D. E. Pritchard, T. A. Savas, and N. Mulders, Phys. Rev. Lett. **97**, 093201 (2006).
[30] A more strongly attractive inverse-square term would generate an infinite dipole series of bound states.
[31] H. Friedrich and A. Jurisch, Phys. Rev. Lett. **92**, 103202 (2004).
[32] E. Mesfin and H. Friedrich, Phys. Rev. A **74**, 032103 (2006).
[33] T. F. O'Malley, L. Spruch, and L. Rosenberg, J. Math. Phys. **2**, 491 (1961).
[34] J. Meixner and F. W. Schäfke, *Mathieusche Funktionen und Sphäroidfunktionen* (Springer-Verlag, Berlin, 1954).
[35] E. del Giudice and E. Galzenati, Nuovo Cimento **38**, 1 (1965).
[36] E. del Giudice and E. Galzenati, Nuovo Cimento **40**, 739 (1965).
[37] L. Bertocchi, S. Fubini, and G. Furlan, Nuovo Cimento **35**, 633 (1965).
[38] F. Arnecke, J. Madroñero, and H. Friedrich, Phys. Rev. A **77**, 022711 (2008).
[39] R. Jost, Helv. Phys. Acta **20**, 256 (1947).
[40] K. Willner and F. A. Gianturco, Phys. Rev. A **74**, 052715 (2006).